Inaugural dissertation
for
obtaining the doctoral degree
of the
Combined Faculty of Mathematics, Engineering and Natural Sciences
of the
Ruprecht - Karls - University
Heidelberg

Presented by
M.Sc. Tamara Steinfass
Born in: Ulm, Germany
Oral examination: 06.10.2022

The influence of secretogranin 2 on the assembly and presentation of the MHC class I complex in melanoma

Referees: Prof. Dr. Viktor Umansky
Prof. Dr. Jochen S. Utikal

Declarations according to § 8 (3) b) and c) of the doctoral degree regulations:

b) I hereby declare that I have written the submitted dissertation myself and in this process have used no other sources or materials than those expressly indicated,

c) I hereby declare that I have not applied to be examined at any other institution, nor have I used the dissertation in this or any other form at any other institution as an examination paper, nor submitted it to any other faculty as a dissertation.

Heidelberg, July 2022

(Tamara Steinfass)

This thesis is dedicated to my family and my friends who always supported me.

Parts of this thesis have been published in:

Conferences and workshop presentations:

- **Tamara Steinfass**, Aniello Federico, Daniel Novak, Jochen Utikal
  Oral and poster presentation: "The role of SCG2 during melanoma progression"
  ADO Nachwuchs Retreat and 29. Deutscher Hautkrebskongress, 2019, Heidelberg and Ludwigshafen, Germany
- **Tamara Steinfass**, Aniello Federico, Daniel Novak, Jochen Utikal
  Poster presentation: "The role of SCG2 during melanoma progression"
  DKFZ PhD Poster Session, November 2020, Heidelberg, Germany
- **Tamara Steinfass**, Daniel Novak, Jochen Utikal
  Poster Presentaion: "The role of SCG2 in melanoma"
  International PhD Student Conference Europe, June 2021, Virtual
- **Tamara Steinfass**, Jochen Utikal
  Scheme Your Project: "The role of SCG2 in melanoma"
  Ph.D. Virtual Retreat, June 2021, Virtual
- **Tamara Steinfass**, Daniel Novak, Giovanni Mastrogiulio, Aniello Federico, Viktor Umansky, Jochen Utikal
  Poster Presentaion: "Secretogranin II (SCG2) influences the assembly and function of MHC class I in melanoma"
  Hallmarks of Skin Cancer Conference (HoSC), November 2021, Virtual

Within the thesis, works from the following publications were included:

- Federico A, **Steinfass T**, Larribère L, Novak D, Morís F, Núñez LE, Umansky V, Utikal J. (2020) Mithramycin A and Mithralog EC-8042 Inhibit SETDB1 Expression and Its Oncogenic Activity in Malignant Melanoma. *Molecular Therapy Oncolytics*.

Contents

Abstract

Melanoma is the reason for the majority of skin cancer-related deaths and reports a rising incidence over the past years. It arises from transformed melanocytes, the melanin-producing skin cells. The primary cause of melanoma is high exposure to ultra violet (UV) radiation. Besides UV radiation, also other factors like genetic predisposition or a weakened immune system can contribute to melanoma development. Depending on the cancer stage, location, and genetic profile different treatment options exist. Gaining new insights into the underlying mechanisms of melanoma progression contributed to the development of new treatment options, such as targeted therapies or immunotherapies. Unfortunately, the development of resistances against treatments negatively influences the therapy success. Therefore, therapy success could be improved through better understanding of the mechanisms leading to therapy resistance and developing potent new therapeutic approaches.

Previous work in our laboratory on the histone methyltransferase SETDB1 (SET domain bifurcated histone lysine methyltransferase 1) revealed a possible role of secretogranin II (SCG2) in melanoma pathogenesis. The results showed that high intratumoral SCG2 expression in melanoma patients correlates with poor survival rates. Based on these data, there was reason to further examine the role of SCG2 in melanoma.

The aim of this project was to investigate the role of SCG2 in melanoma through identifying mechanisms that are influenced by SCG2. First, I could demonstrate that primary melanoma and melanoma metastases show high SCG2 expression levels. By comparing the gene expression levels between SCG2-overexpressing (OE) and control melanoma cells, I found a downregulation of components of the antigen presenting machinery (APM). The components of the APM are important for the correct assembly of the MHC class I complex. Using flow cytometry analysis, I could show that the surface MHC class I levels were downregulated in SCG2 OE melanoma cells. Due to the downregulation of MHC class I, these cells were less sensitive towards cytotoxic T cell-induced killing. The consequences of SCG2 OE on the expression of several APM components, MHC class I surface presentation, and sensitivity towards cytotoxic T cells could be partially reversed by IFNγ treatment.

Taken together, these findings could contribute to the understanding of melanoma immune evasion mechanisms and the role of SCG2 in this process. Consequently, when it comes

to the success of checkpoint blockade and adoptive immunotherapy, SCG2 could be a valuable prognostic factor. Also, new insights into the pathways involved in SCG2-induced MHC class I downregulation could open up new possibilities for melanoma treatment.

Zusammenfassung

Das Melanom ist der Grund für die Mehrzahl der Todesfälle im Zusammenhang mit Hautkrebs und verzeichnet in den letzten Jahren eine steigende Inzidenz. Es entsteht aus transformierten Melanozyten, den melaninproduzierenden Hautzellen. Die Hauptursache des Melanoms ist eine hohe Exposition gegenüber ultravioletter (UV) Strahlung. Neben UV-Strahlung können auch andere Faktoren wie genetische Veranlagung oder ein geschwächtes Immunsystem zur Melanomentstehung beitragen. Je nach Krebsstadium, Lokalisation und genetischem Profil gibt es unterschiedliche Behandlungsmöglichkeiten. Die Gewinnung neuer Einblicke in die zugrunde liegenden Mechanismen der Melanomprogression trug zur Entwicklung neuer Behandlungsoptionen wie zielgerichteter Therapien oder Immuntherapien bei. Leider beeinflusst die Resistenzentwicklung gegen Behandlungen den Therapieerfolg negativ. Daher könnte die Wirksamkeit etablierter Therapien durch ein besseres Verständnis der Mechanismen, die zu Therapieresistenzen führen, und durch die Entwicklung wirksamer neuer Therapieansätze verbessert werden.

Frühere Untersuchungen unserer Arbeitsgruppe zur Histon-Methyltransferase SETDB1 (SET Domain Bifurcated Histone Lysine Methyltransferase 1) deuteten eine mögliche Rolle von Secretogranin II (SCG2) bei der Melanompathogenese an. Die Ergebnisse zeigten, dass eine hohe intratumorale SCG2-Expression bei Melanompatienten mit schlechten Überlebensraten korreliert. Diese Daten veranlassten mich, die Rolle von SCG2 beim Melanom weiter zu untersuchen.

Ziel dieses Projekts war es, den Einfluss von SCG2 auf die Melanompathogenese durch die Identifizierung SCG2-beeinflusster Mechanismen weiter zu untersuchen. Als Erstes konnte ich zeigen, dass primäre Melanome und Melanommetastasen hohe SCG2 Expressionsniveaus aufweisen. Der Vergleich der Genexpressionsniveaus zwischen SCG2-überexprimierenden (OE) und Kontroll-Melanomzellen offenbarte eine Herunterregulierung von Komponenten der Antigen-präsentierenden Maschinerie (APM). Die APM ist wichtig für den korrekten Zusammenbau des MHC Klasse I Komplexes. Mittels Durchflusszytometrie-Analyse konnte ich zeigen, dass die MHC Klasse I Oberflächenpräsentation in SCG2 OE Melanomzellen herunterreguliert war. Aus diesem Grund waren diese Zellen deutlich weniger empfindlich gegenüber induzierter Abtötung durch zytotoxische T Zellen. Die Folgen von SCG2 OE auf die Expression mehrerer APM Komponenten, MHC Klasse I Oberflächenpräsentation und die Empfindlichkeit gegenüber zytotoxischen T Zellen konnten teilweise durch IFNγ-Behandlung umgekehrt werden.

Zusammengefasst könnten diese Ergebnisse zum Verständnis der Immunevasionsmechanismen von Melanomen und der Rolle von SCG2 in diesem Prozess beitragen. Wenn es also um den Erfolg der Checkpoint-Blockade und der adoptiven Immuntherapie geht, könnte SCG2 ein wertvoller Prognosefaktor sein. Außerdem könnten neue Einblicke in die Signalwege, die an der SCG2-induzierten MHC Klasse I Herunterregulierung beteiligt sind, neue Möglichkeiten für die Behandlung von Melanomen eröffnen.

1 List of Figures

2 List of Tables

3 List of Abbreviations

Abbreviation	Meaning
18S	18S ribosomal RNA
A	
ANOVA	analysis of variance
APM	antigen processing and presentation machinery
APS	ammonium persulfate
ATCC	American type culture collection
ATP	adenosine triphosphate
B	
B2M	β2-microglobulin
BCA	bicinchoninic acid protein assay
BRAF	B-RAF proto-oncogene, serine/threonine kinase
C	
CALR	gene encoding calreticulin
CANX	gene encoding calnexin
CDKN2A	cyclin dependent kinase inhibitor 2
cDNA	complementary DNA
CgA	chromogranin A
CgB	chromogranin B
CTLA-4	cytotoxic T lymphocyte associated antigen 4
Ctrl	control
D	
DAPI	2-(4-Amidinophenyl)-1H-indole-6-carboxamidine
DKFZ	German Cancer Research Center
DMEM	Dulbecco's modified eagle's medium
DMSO	dimethyl sulfoxide
DNA	deoxyribonucleic acid
E	
E. coli	Escherichia coli
EDTA	ethylenediaminetetraacetic acid
EMA	European Medicines Agency
ER	endoplasmic reticulum

ERAP	endoplasmic reticulum aminopeptidase
EV	empty vector
F	
FCS	fetal calf serum
FDA	Food and Drug Administration
G	
GAPDH	glyceraldehyde 3-phosphate dehydrogenase
H	
h	hour(s)
HC	heavy chain
HEPES	4-(2-hydroxyethyl)-1-piperazineethanesulfonic acid
HLA	human leukocyte antigen
HRP	horseradish peroxidase
I	
IFN	interferon
IHC	immunohistochemistry
IRF1	interferon regulatory factor 1
J	
JAK	Janus kinase
K	
KD	knockdown
kDa	kilodalton
L	
LAG-3	lymphocyte-activation gene 3
M	
mA	milliampere
MAPK	mitogen-activated protein kinase
MART-1	melanoma antigen recognized by T cells 1
MCA	multiplex cell line authentication
MDSC	myeloid-derived suppressor cells
MEM	modified eagle's medium
MFI	mean fluorescence intensity
MHC	major histocompatibility complex
Min	minutes

mRNA	messenger RNA
N	
NEAA	non-essential amino acids
ns	not significant
NLRC5	NOD-like receptor family CARD domain containing 5
O	
OE	overexpression
OS	overall survival
P	
PBS	phosphate-buffered saline
PD-1	programmed cell death protein 1
PDL-1	programmed cell death ligand 1
Pen-Strep	penicillin streptomycin
PFA	paraformaldehyde
PK	proteinase K
PI	propidium iodide
PVDF	polyvinylidene difluoride
Q	
qPCR	quantitative PCR
R	
RNA	ribonucleic acid
RT	room temperature
S	
SCG2	secretogranin 2
SCG3	secretogranin 3
S.D.	standard deviation
SDS	sodium dodecyl sulfate
SETDB1	SET domain bifurcated histone lysine methyltransferase 1
shRNA	short hairpin ribonucleic acid
SN	secretoneurin
STAT1	signal transducer and activator of transcription
T	
TAMs	tumor associated macrophages
TAP	transporter associated with antigen processing

TAPBP	gene encoding tapasin
TERT	telomerase reverse transcriptase
TGN	trans Golgi network
TMA	tissue microarray
Tregs	regulatory T cells
U	
UTR	untranslated region
UV	ultra violet
V	
V	volt
vs	versus
W	
wt	wild-type

4 Introduction

4.1 Malignant Melanoma

Melanoma is a very aggressive form of skin cancer. The most common form is cutaneous melanoma but it can also occur on mucosal surfaces, in the uveal tract, and leptomeninges [1]. Over the last decades the incidence of melanoma has more than doubled [2]. In 2018, almost 300,000 new melanoma cases were reported with the highest rate in Australia, followed by New Zealand and Norway [3]. Although malignant melanoma just represents 5% of all skin cancer cases it accounts for more than 70% of all skin cancer-related deaths [2]. A major risk factor for the development of melanoma is high exposure to UV radiation and a history of sunburns [4]. Other risk factors include family history of melanoma, gender, age, a weakened immunesystem (e.g. after organ transplantation), and a high number of moles [5, 6]. In general, patients diagnosed with early melanoma stages have good prognosis but about 30% of the patients develop metastases in various organs after primary tumor excision [7]. Despite new therapeutic options, long term prognosis is still poor [2].

4.1.1 Melanoma development and progression

Melanoma arises from transformed melanocytes, the melanin-producing skin cells [8]. Melanocytes originate from the neural crest and migrate for maturation into the epidermis where they gain the ability to produce melanin [9]. Melanin is transported to the neighboring keratinocytes and functions as a natural protection mechanisms against UV radiation since it works as an UV absorbent and antioxidant [10].
Melanocytic transformation is a multi-step process resulting in increased proliferation and morphological changes [11]. This process can be induced by intrinsic factors, such as genetic alterations, or extrinsic factors, like UV radiation [12, 13]. First, a normal melanocyte acquires a driver mutation which can lead to the development of benign melanocytic nevi [14, 15]. One of the most common mutations found is $BRAF^{V600E}$ (B-RAF proto-oncogene, serine/threonine kinase) which is associated with decreased cell proliferation [16]. BRAF-induced nevus development is a cellular protection mechanism preventing malignant transformation of normal cells by the induction of growth arrest, called oncogene-induced senescence [16, 17]. For melanoma development further genetic alterations need to occur [18]. However, most melanomas arise *de novo*, which means that they are not developed from pre-existing nevi lesions [19, 20]. The earliest stage of melanoma is melanoma *in situ*, a precursor stage of invasive melanoma, where the

malignant cells remain restricted to the epithelium and can still be easily resected [21]. Once melanoma cells leave the epithelium and invade the dermis and subcutaneous tissue, melanoma has reached its invasive state [14]. In this stage, melanoma accumulates genetic aberrations (e.g. MAPK (mitogen-activated protein kinase) pathway activation, TERT (telomerase reverse transcriptase) and CDKN2A (cyclin dependent kinase inhibitor 2) mutations) and interacts stronger with the tumor microenvironment consisting of fibroblasts, endothelial cells, immune cells, soluble molecules, and the extracellular matrix. These circumstances result in a more aggressive phenotype [14, 22]. The invasive stage of melanoma is followed by metastatic melanoma where cells of the primary tumor site disseminate to distant sites. Metastases generally first form in the neighboring lymph nodes of the primary tumor, especially the sentinel lymph nodes, whereas distant metastases in visceral tissue occur later [14, 23]. Even though almost all organs can be affected melanoma metastases most frequently occur in the skin, lung, brain, liver, bone, and intestine [8, 24].

4.1.2 Melanoma treatment options

Due to its complexity and heterogeneity malignant melanoma is very aggressive. Therefore, there is a constant need for improvement of existing and development of new treatment strategies. Over the past years, several new therapeutic medications have been approved by the US Food and Drug Administration (FDA) and the European Medicines Agency (EMA), whose application depends on the cancer stage, location, genetic profile, and the condition of the patient [25, 26]. Therapeutic options include surgical resection of the tumor and metastases, chemotherapy, radiotherapy, targeted therapy, and immunotherapy [6, 25].

Surgery

For patients with no metastasizing melanoma, surgical resection of the primary tumor is the primary treatment option. For primary melanoma it is considered as curative in most cases [6]. According to the pathologic features of the tumor, the surgical procedure differs. After evaluation of the excised tumor (thickness and lymph node biopsy) further adjuvant treatment options are considered [25, 27].

Chemotherapy

The earliest treatment option for advanced melanoma was chemotherapy. The drugs used here are the alkylating agents dacarbazine or its prodrug temozolomide, which cause DNA

damage that kills cancer cells. However, these chemotherapeutic drugs do not improve the overall survival (OS) of advanced melanoma patients [25, 27]. Also the combination chemotherapy with cisplatin, a DNA replication inhibitor, vinblastine, a mitotic inhibitor, and dacarbazine does not improve the OS [27, 28]. Therefore, they are used as palliative treatment options for late stage melanoma patients where no other therapeutic options are available [6, 29].

Radiotherapy

Although melanoma is generally considered a radiation-resistant cancer because of its intrinsic DNA damage repair mechanisms, there are some circumstances where radiotherapy is applied. These circumstances include adjuvant treatment after surgical removal of lymph node metastases and palliative treatment in late-stage melanoma [6, 30, 31].

Targeted therapy

The discovery of driver mutations in melanoma enabled the development of therapies targeting the mutated proteins with small molecule inhibitors. The most frequent mutation in melanoma is $BRAF^{V600E}$ leading to a constant activation of the MAPK pathway [16]. This results in increased growth and proliferation of the cancer cells [25]. This hyperactivation can be successfully inhibited by the selective BRAF inhibitors vemurafenib (PLX4032) and dabrafenib (GSK2118436), approved by the FDA in 2011 and 2013, respectively. The application of these drugs led to remarkable response rates and improvement in the OS [25, 32, 33]. Another possibility to target the MAPK pathway is to target MEK1/2, a downstream target of BRAF and NRAS, with trametinib (GSK1120212, approved 2013) or cobimetinib (GDC-0973, XL-518) [25, 34]. Other molecular targets for drug inhibition are the tyrosine-kinase c-KIT (imatinib) and the PI3K-AKT-mTOR pathway (rapamycin, temsirolimus) [27, 32, 34]. For further constant improvement of targeted therapies, the FDA approved combination targeted therapies, which showed greater efficacy than the monotherapies in patients with metastatic melanoma [34–36]. Unfortunately, besides all the promising effects of targeted therapies, patients acquire resistances against the drugs used [37]. The resistance can result from e.g. i) reactivation of the MAPK pathway through further mutations in NRAS or MEK1, or BRAF amplification, ii) modulations in the apoptotic pathway or cell cycle, iii) tumor heterogeneity, iv) alterations in the drug transport system [25, 34, 37, 38]. Therefore, it is important to understand the molecular mechanisms underlying melanoma development and develop novel strategies to overcome drug resistance.

Immunotherapy

Immunotherapy is a treatment approach where the immune system of the patient is directed to the tumor to recognize and eradicate it. The first immunotherapeutic approaches were performed with interferon (IFN) α-2b (FDA approved 1995), peginterferon α-2b (Peg-IFN, approved 2011), and interleukin-2 (IL-2, approved 1998). These cytokines showed immunostimulatory effects but also heavy adverse effects. Despite these adverse effects, cytokine-based immunotherapies are still used in combination with other therapy approaches (ClinicalTrials.gov) [25, 27, 39, 40]. Other immunotherapy approaches target immunosuppressive mechanisms. In 2011, ipilimumab, which acts as an anti-CTLA-4 antibody, was approved by the FDA [25]. Cytotoxic T lymphocyte associated antigen 4 (CTLA-4) is an inhibitory checkpoint receptor that blocks T cell activation and thus helps to keep the balance between immune activation and tolerance [25, 27, 40]. Blocking the inhibitory signal of CTLA-4 through ipilimumab allows cytotoxic T cells to attack the tumor cells [25, 27, 40–42]. Another inhibitory immune checkpoint regulator is programmed cell death protein 1 (PD-1). PD-1 receptor is present on the surface of activated T cells and is activated upon binding to the PD-1 ligands PD-L1 or PD-L2 present on the surface of various cancer cells. Interaction of PD-1 with its ligand PD-L1/2 leads to T cell suppression [25, 27, 40, 43]. The anti-PD-1 antibodies nivolumab (approved 2014) and pembrolizumab (approved 2015) inhibit the interaction between PD-1 and PDL-1/2 and lead to an immune response and anti-tumor activity reducing tumor progression, with relative mild adverse effects [25, 27, 34, 40, 43–46]. Recently (in 2022), the FDA approved the combination treatment of nivolumab and relatlimab, a lymphocyte-activation gene 3 (LAG-3) inhibitory antibody [47]. LAG-3 is expressed on the cell surface of immune cells, including activated T cells, and negatively influences T cell function and CD4 T cell activation [48–50]. The combination treatment of relatlimab and nivolumab significantly improved the median progression-free survival compared to nivolumab monotherapy. This study validates the inhibition of LAG-3 as the third immune checkpoint inhibition with clinical benefit [51]. Other immunotherapy options are oncolytic virus therapy (approved 2015), development of vaccines (gp100 peptide, toll-like receptor (TLR) agonists), and adoptive T cell therapy (administration of melanoma-specific T cells) [52–55].

4.1.3 Melanoma immune evading mechanisms

It is known that cancer cells permanently adapt to the host defense mechanisms by pathway alteration. Hanahan and Weinberg divided these cancer abilities into several categories of adaptation mechanisms called "The Hallmarks of Cancer": maintaining prolifer-

ative signaling, inducing angiogenesis, escaping growth suppressors, enabling replicative immortality, resisting cell death, activating invasion and metastasis, deregulating cellular energetics, tumor-promoting inflammation, genome instability and mutation, and avoiding immune destruction [56]. During the last years, studying the mechanisms of immune evasion more and more became the focus of attention. Also in melanoma immune evading pathways have been discovered. The microenvironment of melanoma contains a great number of immune-suppressive immune cells like regulatory T cells (Tregs), myeloid-derived suppressor cells (MDCS), and tumor-associated macrophages (TAMs) [6]. $CD4^+$ Tregs, under normal conditions, help to prevent damage to the host by an overactive immune response [6, 57]. This immune suppressing effect of Tregs can be induced by (i) release of inhibitory cytokines, (ii) induction of cytolysis, (iii) metabolic disruption of immune cells, and (iv) targeting dendritic cells in their maturation and/or function [6,57,58]. Other cells in the melanoma microenvironment are MDSCs. These cells originate from myeloid cells which are found in the bone marrow and are a major component of the innate immune system. They protect the host from pathogens by phagocytosis and the secretion of inflammatory cytokines [6,59]. An increase in MDSCs leads to melanoma progression, reduced cytotoxic T cell function, and can be used as a prognostic factor [60–62]. Another significant component of the melanoma microenvironment are TAMs which develop from monocytes and exert immunosuppressive functions like the expressing immune checkpoint modulators and producing immunosuppressive chemokines and matrix metalloproteinases [63–66].

Besides the immunosuppressive function of components of the melanoma microenvironment, also dysregulation of pathways involved in activating cytotoxic T cells contributes to an immunosuppressive milieu. One of this pathways is the antigen processing and presentation by the major histocompatibility complex class I [9].

4.2 Major histocompatibility complex (MHC) class I

The major histocompatibility complex (MHC) class I plays an important role in the immune system [67]. It is present in all nucleated cells and its purpose is to present intracellular peptides on the cell surface, which are recognized by $CD8^+$ T cells leading to their activation [67, 68]. MHC class I molecules consist of one heavy chain (HC) and the invariable light chain β2-microglobulin (B2M) [69]. The extracellular part of the HC folds into three domains called α1, α2, and α3, where the α1 and α2 domains form the peptide-binding cleft and the α3 domain anchors the molecule to the plasma membrane (Fig. 1) [70, 71]. In most vertebrate species, the HCs are encoded by three genes, which

are highly polymorphic. In humans these three genes are HLA-A, HLA-B, and HLA-C (HLA; human leukocyte antigens) [68]. The polymorphism of these genes affects the composition of the peptide-binding groove and thus influences the variety of peptides presented to $CD8^+$ T cells on the cell surface [67].

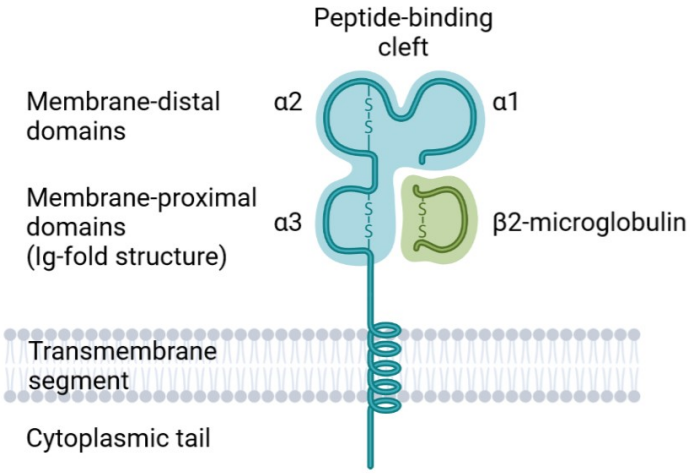

Fig. 1: Schematic representation of the MHC class I complex.
The heterodimeric MHC class I molecule consists of a heavy chain (HC) and an invariable light chain; β2-microglobulin. The extracellular part of the HC folds into three domains (α1, α2, α3) encoded by the HLA genes. The α1 and α2 domains form the peptide-binding cleft while the α3 domain anchors the molecule to the plasma membrane. Figure adapted from Schumacher et al., *Proteomics* [71].

4.2.1 MHC class I antigen processing and presentation

The process that leads tot he presentation of proteins by MHC class I can be divided into 4 steps, as can be seen in Fig. 2: 1) peptide generation by proteasomes and trimming by peptidases, 2) transport of the peptides to the endoplasmic reticulum (ER), 3) assembly of the MHC class I complex and peptide loading, and 4) antigen presentation via MHC class I on the cell surface [72].

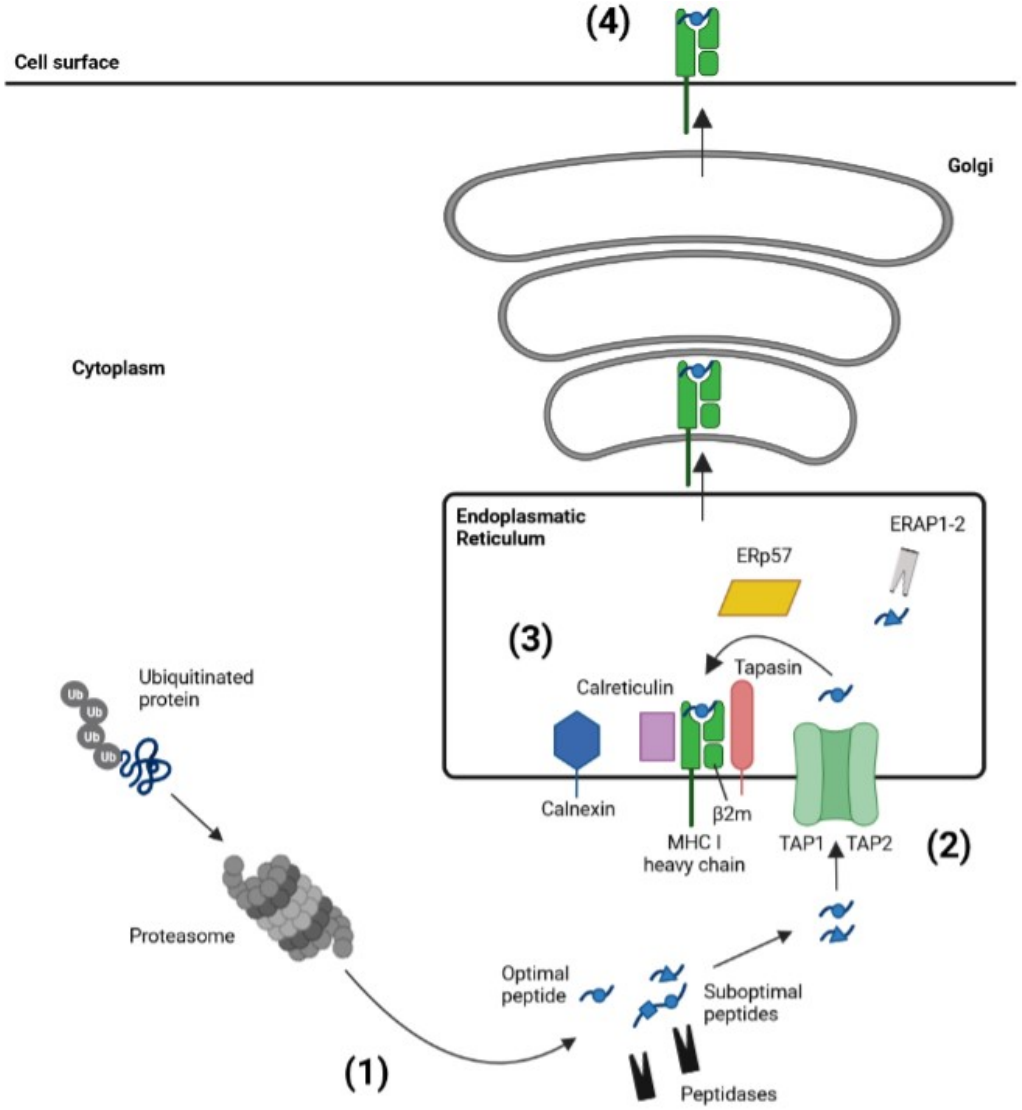

Fig. 2: MHC class I complex assembly and antigen presentation in four steps.
The process of MHC class I assembly and antigen presentation on the cell surface can be divided into four steps: (1) peptide generation through proteasomal degradation and further peptide trimming by peptidases, (2) peptide transport into the the ER by TAP1 and TAP2, (3) loading of optimally trimmed peptides onto MHC class I molecules with the help of tapasin, calreticulin, ERp57 and calnexin or further trimming of suboptimal peptides by ERAP1-2, and (4) antigen presentation via MHC class I on the cell surface. Figure adapted from Leone et al., *JNCI* [72].

Peptide generation and trimming

Under normal cellular conditions, proteins undergo a permanent turnover of degradation and new synthesis. Two different proteolytic pathways are responsible for the degradation of most proteins: the lysosomal pathway and the ubiquitin-proteasome pathway [72, 73]. The peptides generated in the ubiquitin-proteasome pathway are presented by MHC class I molecules [72, 74]. Proteins degraded through this pathway include cytosolic proteins

like short-lived regulatory proteins, and damaged, misfolded, mutated, or virus-derived proteins [72, 75–77]. To target these proteins for degradation through the ubiquitin-proteasome pathway, they are tagged with multiple copies of ubiquitin to a free amino group of a lysine residue [72]. These ubiquitinated proteins pass through the activated proteasome where they unfold, spread along the proteasome, and are deubiquitinated. Then, these proteins are cleaved within the proteasome into peptides ranging from 2-25 residues and released into the cytosol [68,72]. These cytosolic peptides are further cleaved by enzymes in the ER, to fit into the peptide-binding groove of MHC class I complex molecules [72,78–80]. One of these enzymes is ERAP1 (Endoplasmic reticulum aminopeptidase 1), an ER aminopeptidase. Because of its substrate preference it is determined as a "molecular ruler" [81]. ERAP1 spares the peptides of 8-9 residues, which is the typical size for MHC class I binding, and trims peptides of 9-16 residues [72, 81]. ERAP1 preferentially trims peptides with hydrophobic C-termini and is induced by IFNγ [81,82].

Peptide transport into the ER

After their generation in the cytosol by proteasomes, peptides are transported into the ER by the ATP-dependent TAP complex (transporter associated with antigen processing) [83–85]. It is a heterodimeric complex composed of TAP1 and TAP2, which both belong to the ATP-binding cassette transporter family [72,86]. The transmembrane pore in the ER membrane, which is formed by TAP1 and TAP2, opens and closes depending on ATP binding and hydrolysis [72, 83, 84, 87]. TAP most efficiently transports peptides with a length of 9-16 residues [81, 88]. Peptides, which are too long and therefore do not fit into the MHC class I binding groove, can be cleaved in the ER lumen or are transported back into the cytosol where additional trimming is performed by cytosolic peptidases. Afterwards these peptides can be transported back into the ER in a TAP-dependent manner and are loaded onto MHC class I molecules [72, 89].

Peptide loading onto MHC class I

After the transport of the petides through the TAP complex into the ER, the peptides associate with nascent MHC class I molecules and B2M [69,72]. This is facilitated with the help of the chaperone proteins tapasin, calnexin, calreticulin, and the thiol oxidoreductase ERp57 [72, 90]. These chaperones together with TAP and MHC class I molecules form the peptide loading complex (PLC) [72]. Newly synthesized MHC class I HC located in the ER carry a $Glc_1Man_9GlcNAc_2$ glycan which is recognized by calreticulin and calnexin [72, 91, 92]. MHC class I HC interacts with calnexin, which together with ERp57 ensures correct folding and oxidation of the HC and therefore enables the binding of B2M to the

HC [72, 90, 93–95]. The binding of B2M leads to the release of calnexin resulting in a conformational change that creates an "open" form of the HC/B2M heterodimer, which is highly unstable [72,90,95]. The dimer is stabilized by the binding of tapasin, calreticulin, ERp57, and TAP [72, 90, 96]. Tapasin connects MHC class I molecules to TAP, which transports the peptides, destined to be loaded onto empty MHC class I molecules, into the ER [72, 90, 96, 97]. Additionally, tapasin is indispensable for the stabilization of the HC/B2M heterodimer and for optimized peptide loading [72, 98–100]. The interworking proteins, multimeric protein complexes, and organelles mentioned above represent the MHC class I antigen processing and presentation machinery (APM) [72].

Antigen presentation

After successful loading of the peptide into the MHC class I groove, the chaperones are released and the MHC class I-peptide complex is packed into vesicles. These vesicles exit the ER, are transported through the Golgi apparatus, and migrate to the cell membrane. Arriving at the cell membrane, the vesicular membrane fuses with it. This fusion results in the presentation of the MHC class I-peptide complex to the extracellular space, where it can be recognized and bound by the T cell receptor of $CD8^+$ T cells. $CD8^+$ T cells are important for the eradication of intracellular pathogens and also have antitumoral function [72]. Therefore, impaired expression and function of the APM components can contribute to tumor development and progression [101, 102].

4.2.2 MHC class I in cancer

MHC class I presents peptides processed within the cell as antigenic information on the cell surface. This enables $CD8^+$ T cells to identify cells expressing abnormal proteins, such as cancer cells. Therefore, there is a need for cancer cells to avoid elimination by $CD8^+$ T cells in order to survive. Since MHC class I molecules are not necessary for cell survival, a mechanism of cancer cells to escape immune control is to lose the APM. This will not only impair the natural immune response but also affect immunotherapies, such as checkpoint-blockade, that require the stimulation of $CD8^+$ T cells [101].
Many different human cancer types have been reported to lose MHC class I molecule expression including non-small cell lung, breast, prostate, and colorectal cancer, hepatocellular carcinoma, head and neck squamous cell carcinoma, and melanoma [101]. Since MHC class I molecules alone are very unstable without chaperone- or peptide-binding and held back in the ER, defects in the MHC class I pathway can occur during every step of the assembly (e.g. proteasome, TAP, tapasin, ERp57, B2M) leading to loss of sur-

face MHC class I [101]. Specifically in melanoma, defects in proteasomal subunits, TAP1 and TAP2, ERAP1 and ERAP2, and tapasin, as well as total loss of MHC class I have been reported [72,103–114]. The deregulation of immunoproteasome subunits, TAP1 and TAP2, as well as tapasin in melanoma has been found to be associated with defective IFNγ signaling [108]. Also in melanoma, IFNγ signaling correlates with the response to immunotherapy [101, 115].

In all cells, MHC class I component expression and surface presentation can be restored upon stimulation with IFNs, especially IFNγ [101, 116]. Under normal conditions, IFNs are produced in response to infections and T cell responses to increase the possibility to eradicate pathological cells [101]. IFNs bind to their receptor and stimulate the phosphorylation of JAK1 and JAK2 (Janus kinases). In turn, JAK1 and JAK2 phosphorylate the transcription factor STAT1 (Signal transducer and activator of transcription 1). Phosphorylated STAT1 translocates into the nucleus and triggers the transcription of NLRC5 (NOD-like receptor family CARD domain containing 5) and IRF1 (interferon regulatory factor 1) by binding to their promoter elements. NLRC5 and IRF1 then induce the MHC class I APM gene transcription [101].

There is also potential to restore APM gene expression in tumors, where APM genes are structurally intact but their expression is downregulated [101]. Studies showed that MHC class I levels can be increased upon IFNγ treatment [117–119]. There exist recombinant type I and II IFNs that are approved by the FDA and work *in vivo* [101]. In a small phase 2 trial, systemic administration of IFNγ induced MHC class I expression in two patients with MHC class I negative melanoma [101,118]. Additionally, in a clinical trial in melanoma, IFNγ administration improved the outcome of checkpoint blockade therapy. However, it is not known to what extent this was due to MHC class I expression [101,120].

For cancers, where APM genes are not structurally intact due to deletions or inactivating mutations in structural antigen presenting genes, e.g. β2-microglobulin, gene replacement would be required to restore MHC class I presentation [101, 121–123]. For restoring MHC class I antigen presentation in cancers that have activated epigenetic silencing mechanisms, these repressive epigenetic marks needs to be reversed [101, 113, 124, 125]. Also microRNAs can reduce MHC class I antigen presentation and are therefore a possible therapeutic target [101, 126, 127]. Furthermore, inhibition of enzymes leading to the loss of MHC class I antigen presentation could be another option of restoring MHC class I antigen presentation [101, 128–130]. Studying the various mechanisms that can lead to the loss of MHC class I antigen expression and the identification of potential therapeutic targets to reverse this loss are crucial to restore immune control and improve T cell-based

immunotherapy [101].

4.3 Secretogranin 2 (SCG2)

SCG2 is also called chromogranin C. Its gene is located on chromosome 2q35-2q36 and includes 2 exons, where exon 1 encodes 215 nucleotides of the 5'-UTR and exon 2 14 nucleotides of the 5'-UTR, the entire coding region as well as the 3'-UTR [131, 132]. SCG2 has a size of 71 kDa and is synthesized as a 617-amino-acid preproprotein. It can be endoproteolytically cleaved by prohormone convertases at 9 different sites characterized by two sequential basic amino acids. This results in intermediate-sized proteins and the bioactive peptides secretoneurin (SN), EM66, and manserin (Fig. 3) [131, 133–135]. Together with chromogranin A (CgA) and B (CgB), SCG2 belongs to the granin family [136–138]. These proteins are part of the neuroendocrine system and play a crucial role in secretory granule formation and biogenesis [131, 136, 138]. Chromogranins and Secretogranins have many characteristics in common, which include an acidic isoelectric point, the ability to bind calcium, the tendency to form aggregates, and they carry many dibasic cleavage sites. Besides CgA, CgB, and SCG2, also other granin family members exist: SCG3 (secretogranin 3), 7B7, NESP55, VGF, and ProSAAS. Many of these proteins are synthesized as precursors of biologically active peptides which are part of a broad range of different pathways ranging from pain and inflammatory pathways, over metabolic and mood disorders, to blood pressure regulation [131].
Granins, as SCG2, are synthesized at the rough ER and transported into the ER cisternae through a N-terminal signaling sequence. Afterwards, granins are transported from the ER to the Golgi through transport vesicles [131, 139]. In the TGN (trans Golgi network) they are packed, together with prohormones and their corresponding processing enzymes, into immature granules. Within these immature granules, granins are partially processed into biologically active peptides. After maturation of the immature granules, they are stored and released upon stimulation [131, 140]. An important step in the sorting process of granins into secretory granules is the formation of aggregates in the TGN. After aggregation, membrane binding proteins bind to the sorting signals on the granins for correct sorting [131, 141–143]. It has been shown that SCG2 has targeting signals at the C- and N-terminus, which can act independently and each of them is sufficient to sort SCG2 into secretory granules in PC12 cells [131, 143]. It also has been found that SCG2 can bind to SCG3, which raises the posibility that SCG2 is sorted into secretory granules via TGN membrane-anchored SCG3 [131, 144]. Besides its role in the formation of secretory granules, SCG2 also plays a role as a biomarker in cardiovascular diseases and hypertension,

inflammatory diseases, neurodegenerative and neuropsychiatric diseases, and also some cancer types [131].

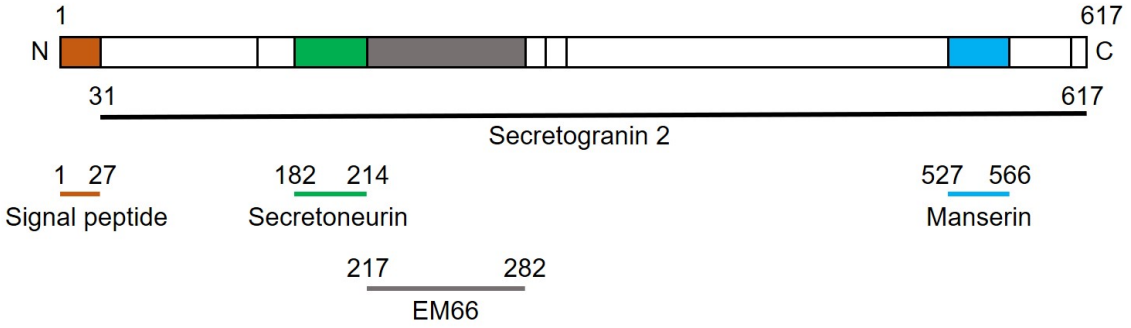

Fig. 3: Schematic representation of SCG2 protein structure and active peptides.
Black line represents full length secretogranin 2 protein; orange square, the signal peptide; green square, secretoneurin; grey square, EM66; blue square, manserin. N, N-terminus; C, C-terminus. Figure adapted from Montero-Hadjadje et al., *Acta Physiol (Oxf)*; Guillemot et al., *J Mol Endocrinol*; and UniProt (https://www.uniprot.org/uniprot/P13521, accessed March 2022.) [137, 145].

4.3.1 SCG2 in cancer

The proteolycally processed peptides of SCG2 can be used to identify endocrine tumors. SN, for example, is considered a specific marker for pancreatic tumors, and EM66 helps to discriminate benign from malignant pheochromocytoma [131, 146–148]. For neuroblastoma cells it was found that SCG2 protects them from nitric oxide-induced apoptosis [149]. In colorectal cancer, high expression of five stroma-related genes including SCG2 was associated with poorer survival of the patients [150]. In another study a five-gene signature including SCG2 was identified as a prognostic factor in colorectal cancer. Patients with a high expression of this five-gene signature showed a poorer survival compared to patients with a lower expression [151]. On the other hand, a recent study in colorectal cancer showed that ectopic SCG2 expression inhibits colorectal cancer tumor growth in mice and therefore it is suggested to use SCG2 expression in colorectal cancer tumor cells as a positive prognostic marker [152]. In the same study, it was also found that SCG2 inhibits tumor angiogenesis, although this finding was inconsistent with previous studies on endothelial cells [152–154]. The role of SCG2 in prostate cancer was also addressed in several studies revealing a correlation between SCG2 expression levels and prostate cancer progression as well as an increased proliferative behavior [136]. Additionally, in melanoma it has been found that SN, the cleavage product of SCG2, plays a role in the induction of a more migratory behavior [155]. Another, more recent study on melanoma discovered that SCG2 accumulated in vesicle-like structures in the perinuclear region upon SCG2 over-

expression, which might lead to an activation of the secretory machinery resulting in the secretion of protumorgenic factors. In the same study it could also be shown that SCG2 might be a prognostic factor in melanoma, since SCG2 expression was highly increased in clinical samples belonging to patients with metastases and low survival rate [156]. Based on these previous findings, the role of SCG2 seems to be cancer and cell type-specific. Therefore, it is important to further study the role of SCG2 in cancer.

5 Research Objective

In this thesis, I aimed at investigating the SCG2-driven mechanisms in melanoma, with particular emphasis on the role of SCG2 in MHC class I assembly and presentation.

In more detail, my aims were to:

- Evaluate the influence of SCG2 on melanoma patient survival and to compare its expression between normal skin and melanoma.
- Investigate the role of SCG2 in melanoma progression with the focus on cell cycle analysis.
- Examine the influence of SCG2 on the expression of some components of the APM and subsequently on the cell surface levels of the MHC class I complex and to see if this has an influence on the sensitivity towards cytotoxic T cells.

6 Materials

6.1 Reagents and Kits

Product	**Company**	**Catalog No.**
Adhesive clear qPCR seals	Biozyme	600238
Agarose NEEO Ultra Quality	Carl Roth	2267.4
Ampicillin	Carl Roth	HP62.1
BSA-Powder, Albumin Fraction V	Carl Roth	8076.2
BstBI (10 U/L)	Thermo Fisher Scientific	IVGN0886
cOmplete Mini Protease Inhibitor Cocktail	Roche Diagnostics	04693159001
DAPI	Roche	10236276001
DH5α Competent Cells	Thermo Fisher Scientific	18265017
Endofree Plasmid Maxi Kit	Qiagen	12362
Immobilon PVDF (polyvinylidene difluoride) membrane, 0.45µM	Merck Millipore	IPVH00010
LB-Medium	Carl Roth	X964.2
Luminata Forte Western HRP Substrate	Merck Millipore	WBLUF0500
Midori Green Advance	Nippon Genetics	mg-04
NuPage™ gels 4-12% Bis-Tris Protein,1 mm x 10 well	Invitrogen	NP0321BOX
NuPage™ gels 4-12% Bis-Tris Protein,1 mm x 15 well	Invitrogen	NP0323BOX
NuPage™ LDS Sample Buffer (4x)	Thermo Fisher Scientific	NP0008
NuPAGE™ MOPS SDS Running buffer (20x)	Invitrogen	NP0001

NuPage™ Sample Reducing Agent (10x)	Thermo Fisher Scientific	NP0004
O'GeneRuler 1 kb DNA Ladder	Thermo Fisher Scientific	SM1163
O'GeneRuler 100bp DNA-Ladder	Thermo Fisher Scientific	SM1143
PageRuler Plus Prestained Protein Ladder	Life Technologies	26619
Paraformaldehyde	Sigma-Aldrich	P6148-1KG
Pierce BCA Protein Assay Kit	Thermo Fisher Scientific	23225
Platinum Taq Polymerase	Thermo Fisher Scientific	10966034
Propidium iodide (PI)	BD Biosciences	51-66211E (sold as 556463)
Proteome Profiler Human Cytokine Array Kit	R&D systems	ARY005B
PhosSTOP™ Phosphatase inhibitor Cocktail	Roche Diagnostics	04906845001
Qiaprep Spin Miniprep Kit	Qiagen	27106
Recombinant Human IFNγ	Peprotech	AF-300-32
Restore™ PLUS Western Blot Stripping Buffer	Thermo Fisher Scientific	46430
RevertAid First strand cDNA Synthesis Kit	Thermo Fisher Scientific	K1622
RIPA	Sigma-Aldrich	R0278
Rnase-Free Dnase Set	Qiagen	79254
RNeasy Plus Mini Kit	Qiagen	74136
Skim milk powder	Gerbu Biotechnik	1602,1000
SOC Outgrowth Medium	New England BioLabs	(B9020S)
SYBR Green PCR Master Mix	Applied Biosystems	4309155
T4 Ligase	Life Technologies	EL0011
TritonX-100	Carl Roth	3051.4
Tween® 20	Merck	10017805

Qiaprep Spin Miniprep Kit	Qiagen	12583
Venor Gem Classic Myco PCR Kit	Minerva Biolabs	11-1100
XhoI (10 U/L)	Thermo Fisher Scientific	ER0691
X-treme GENE® 9 DNA Transfection Reagent	Roche Diagnostics	06365787001

6.2 Reagents for cell culture

Product	**Company**	**Catalog No.**
2-Mercaptoethanol	Gibco®Life Technologies	31350010
Blasticidine	Sigma-Aldrich	15205
Dimethyl sulfoxide (DMSO)	Carl Roth	A994.2
Dulbeccos's Modified Eagle Medium (DMEM), high glucose	Gibco®Life Technologies	41965-039
Fetal Calf Serum (FCS)	Biochrom	S0115
IFNγ	Peprotech	AF-300-02
Non-essential amino acids (NEAA)	Sigma-Aldrich	M7145
Phosphate-buffered saline (PBS)	Sigma-Aldrich	D8537
Penicillin/Streptomycin	Sigma-Aldrich	P4333
Polybrene Infection/Transfection Reagent	Sigma-Aldrich	TR-1003-G
Puromycin	Carl Roth	240.1
Trypan blue solution	Sigma-Aldrich	93595
Trypsin-EDTA	Sigma-Aldrich	T3924

6.3 Human cell lines

Cell line	**Source**	**Cell type**	**Mutation**
C32	ATCC	Melanoma cell line	BRAF V600E
HEK293T	ATCC	Embryonic kidney cells	WT
HT144	ATCC	Melanoma cell line	BRAF V600E

T cells (MART-1-specific)	Provided by the Joint Immunotherapeutics Laboratory, German Cancer Research Center (DKFZ), Heidelberg. Generated according to Johnson et al., *J Immunol* [157].	T cell line	-
WM266-4	ATCC	Melanoma cell line	BRAF V600D

6.4 Antibodies

Specificity	**Source**	**Company**	**Catalog No.**
Anti-rabbit IgG, HRP-linked antibody	goat	Cell signaling	7074
APC anti-human HLA-A,B,C antibody	mouse	BioLegend	311410
B2M (D8P1H)	rabbit	Cell signaling	12851
Calnexin (C5C9)	rabbit	Cell signaling	2679
Calreticulin (D3E6) XP®	rabbit	Cell signaling	12238
Chromogranin C (SCG2)	rabbit	GeneTex	GTX54665
GAPDH (14C10)	rabbit	Cell signaling	2118
Stat1 (D1K9Y)	rabbit	Cell signaling	14994
pStat1 (Y701) (D4A7)	rabbit	Cell signaling	7649
TAP1 (E4T4F)	rabbit	Cell signaling	49671
TAP2	rabbit	Cell signaling	12259

Tapasin (E6P2Z) XP®	rabbit	Cell signaling	66382

6.5 Plasmids

Name	Source
pCMV-dR8.91 (Packaging)	Konrad Hochedlinger (Harvard, Boston, USA)
pCMV-VSV-G (Envelope)	Addgene No.8454
pLEX980 empty vector	obtained from pLEX980-hSCG2 by removing hSCG2
pLKO.1-puro non-targeting	Addgene No.1864
pLEX980-hSCG2	obtained from pLEX980-SETDB1 (obtained from Craig Ceol, Children's Hospital Boston, USA) by replacing SETDB1 with human SCG2 (NM_003469, SC117954, ORIGENE)
SCG2 shRNA	TRCN0000055605 (Sigma-Aldrich)

6.6 Primers

Amplification target	Forward Sequence	Reverse Sequence
B2M	GAGGCTATCCAGCGTACTCCA	CGGCAGGCATACTCATCTTTT
CALR	CCTGCCGTCTACTTCAAGGAG	GAACTTGCCGGAACTGAGAAC
CANX	CCAAGGTTACTTACAAAGCTCCA	GGCCCGAGACATCAACACA
SCG2	AGCCGAATGGATCAGTGGAA	GATGGTCTAAGTCAGCCTCTGAGA
STAT1	ATCCTCGAGAGCTGTCTA	GCCAGGTACTGTCTGATT
TAP1	CTGGGGAAGTCACCCTACC	CAGAGGCTCCCGAGTTTGTG

TAP2	CACCTACACCATGTCTCGAATC	AGTTACTCATCAGGGTGGTATCC
TAPBP	TGGACCGGAAATGGGACC	CCCCAGAAGGGTAGAAGTGG
18S	GAGGATGAGGTGGAACGTGT	TCTTCAGTCGCTCCAGGTCT

6.7 Solutions and Buffers

Name	**Composition**
Blocking Buffer (BSA)	5% BSA 1x TBST
Blocking Buffer (milk)	5% Skim milk powder 1x TBST
Cell freezing medium	80% FCS 20% DMSO mixed 1:2 with MEF medium
Cell lysis buffer for protein isolation	1x PhosSTOP 1x cOmplete mini protease inhibitor cocktail RIPA
FACS Buffer	PBS 1% BSA 0.05% sodium azide
LB medium	20g LB-Medium 1l H_2O
MEF medium	DMEM+GlutaMAXX 10% FCS 1% penicillin/streptomycin 1% NEAA 0.1 mM 2-Mercaptoethanol
10x TBS (pH 7.6)	150mM NaCl 50mM Tris dH_2O

Transfer Buffer (pH 8.3)	25mM glycine 190mM Tris 20% SDS 20% methanol dH_2O
Washing Buffer (1x TBST)	0.02% Tween® 20 1x TBS

6.8 Equipment

Product	**Company**
15 ml and 50 ml Tubes	Falcon
6 Well Multi Well Plates	Greiner Bio-One
5, 10, 25 ml Pipettes	Corning
8 Well Culture Slide	Falcon
AB 7500 Real-Time PCR Machine	Applied Biosystems
CELLSTAR® Cell Culture Flask	Greiner Bio-One
Centrifuge 5810 R	Eppendorf
ChemiDoc™ Touch Imaging System	Bio-Rad
Cryotubes, 1,8 ml external thread	Thermo Fisher Scientific
FacsCanto II	BD Biosciences
Facs Tubes	NeoLab
Hemocytometry	Neubauer
Leica DM LS light microscope	Leica
LSR Fortessa HTS	BD Biosciences
MicroAmp Optical 96 Well Plate qPCR	Thermo Fisher Scientific
Microplates 96 Well	Falcon
Nanodrop Spectophotometer ND-1000	Peqlab Biotechnologie GmbH
Nikon Eclipse Ti Fluorescence Microscope	Nikon
Rotilabo®-syringe filters, 0,22 µm	Carl Roth
Rotilabo®-syringe filters, 0,45 µm	Carl Roth
Table Centrifuge 5418 R	Eppendorf

Tecan Infinite F200 PRO	Tecan
Thermomixer compact	Eppendorf
xCELLigence E-Plate 96 PET	Agilent
xCELLigence RTCA MP analyzer	ACEA Bioscience
xCELLigence RTCA MP workingstation	ACEA Bioscience

6.9 Software tools

Name	**Source**
7500 Software v2.0.5	Applied Biosystems
ApE	M. Wayne Davis (Open Source)
Aperio ImageScope 12.1	Aperio Technologies
Chipster	Chipster Open source
EndNote	Clarivate Analytics
FlowJo 7.2.2	FlowJo
GraphPad PRISM	GraphPad software
i control 1.10	TECAN
ImageJ	National Institute of Health
Image Lab™ Software 6.0.1	BioRad
Microsoft Office 2019	Microsoft
NDP.view 2	Hamamatsu
NIS-Element	Nikon
TexMaker	Pascal Brachet

7 Methods

7.1 Cell Culture

All cell lines were cultured in DMEM (Gibco, Life Technologies) containing 10% heat-inactivated FCS (Biochrom), 1% penicillin/streptomycin (Sigma-Aldrich), 1% NEAA (Sigma-Aldrich), and 0.1 mM β-mercaptoethanol (Gibco, Life Technologies). Cells were stored in an incubator with 37°C, 5% CO_2, and 95% humidity.
Experiments were performed when cells reached about 80% confluency. Firstly, cells were washed with PBS (Sigma-Aldrich) to remove debris and dead cells followed by trypsinization with trypsin-EDTA (Sigma-Aldrich). Next, detached cells were stained with trypan blue solution (Sigma-Aldrich) and viable cells were counted with a hemocytometer counting chamber. Afterwards, cells were seeded at specific densities according to the experiment planned. For long term storage, cells were resuspended in freezing medium (FCS + 20% DMSO) and stored at -80°C or in liquid nitrogen. Cell identity was verified using a multiplex cell line authentication test (MCA; Multiplexion GmbH). Also, cells were tested for mycoplasma contamination on a regular basis using Venor®GeM Classic Mycoplasma detection kit (Minerva Biolabs).

7.2 IFNγ stimulation

One day before treatment 2x10^5 cells/well were seeded in a 6 well plate. The next day, cells were treated with 10 ng/ml IFNγ. After 24h, cells were treated again and 48h after the first treatment cells were harvested.

7.3 Transduction with lentiviral particles

For lentiviral particle production HEK293T cells were used. Before transfection, cells were grown to a density of 60%. For transfection, 11 µg of the plasmid of interest were mixed with the packaging plasmids pCMV-VSV-G (5.5 µg), pCMV-dR8.91 (8.25 µg), and X-treme GENE® (Roche) solution in pure DMEM. The mixture was added to the HEK293T cells after 30 min of incubation at room temperature (RT). After 12h, supernatant was discarded and new medium was added. After 24, 36, and 48h supernatant containing lentiviral particles was collected and filtered through a 0.45 µm PVDF filter (Carl Roth). The virus suspension was used to infect melanoma cells or stored at -80°C. For infection, melanoma cells were cultured in transduction medium containing 50% medium and 50% virus suspension. To increase the transduction efficiency, 8 µg/mL

polybrene (Sigma-Aldrich) were added. After 24h, cells were re-infected with new transduction medium without adding polybrene. 48h after the first infection, cells were washed three times with PBS and cultured in their culturing medium. In order to remove the non-transduced cells, cells were selected in medium containing 0.5-1 µg/mL puromycin (Carl Roth) or 10-15 µg/mL blasticidine (Sigma-Aldrich) according to the resistance gene. Cells were selected for about 3 days until non-transduced control cells completely died. According to the safety instruction, lentivirus production, collection, storage, and infection of cells were performed in a biosafety level II laboratory.

7.4 Western Blot

For protein extraction, cells were harvested and washed once with PBS. Cells were then resuspended in RIPA buffer containing 1x Complete Mini Protease Inhibitor Cocktail (Roche) and 1x of PhosphoSTOP (Roche). Cells were lysed for 30 min on ice and afterwards centrifuged for 20 min at 15000 rpm and 4°C. Supernatant containing isolated proteins was collected and stored at -80°C. Protein concentrations were determined using Pierce BCA Protein Assay Kit (Thermo Fisher Scientific), according to manufacturer's instructions.
Depending on the protein concentration, 20-30 µg protein were loaded onto NuPAGE™ Novex™ 4-12% Bis-Tris Protein gels (Thermo Fisher Scientific) to separate proteins by size via electrophoresis. After the run, proteins were transferred onto PVDF membranes (Merck Millipore). Then, membranes were blocked in 5% milk or 5% BSA for 1h at RT to avoid unspecific binding of the antibodies. Subsequently, membranes were incubated with specific primary antibodies, diluted in the blocking buffer, over night at 4°C on a shaker. The following day, membranes were washed three times with 1x TBST to remove excess of primary antibody. Then, membranes were incubated with the suitable HRP-conjungated secondary antibody diluted in the blocking buffer for 1h at RT. For protein detection, membranes were washed again three times with 1x TBST and then exposed to Luminata Forte western HRP substrate (Merck Millipore). Images were acquired using ChemiDoc™ Touch Imaging System (BioRad) and analyzed by ImageJ software (NIH) and Image Lab (BioRad).

7.5 Tissue microarray (TMA) staining

Human tissue samples from healthy donors and melanoma patients were processed to TMA samples as previously described in Wagner et al., 2015 [158]. Tissue samples were

stained with antibodies against SCG2. As a positive control, TMAs were stained with an antibody against S100β. For digitalization, stained TMAs were scanned by the NCT-Gewebebank facility at the pathology unit, University of Heidelberg. The sections were examined independently by two persons, which scored the images according to the immunohistochemistry score system (score range: 0–12) [158]. Declaration of consent was performed based on the ethical votes 2010-318N-MA and 2014-835R-MA (ethics committee II of Heidelberg University, Germany) and was received from all patients included in the study.

7.6 Ribonucleic acid (RNA) isolation

For RNA isolation, cells were harvested and washed once with PBS. Total RNA was isolated using RNeasy Mini Kit (Qiagen), according to manufacturer's instructions. To avoid contaminations with genomic DNA, an on-column DNase digest was performed using RNase-Free DNase (Qiagen) for 15 min at RT. Quality and concentration of the RNA were determined with NanoDrop ND1000 spectrophotometer (PEQLAB Biotechnologie GmbH, Erlangen, Germany).

7.7 Complementary DNA (cDNA) synthesis and real time quantitative PCR (qPCR)

For cDNA synthesis, 500 ng of total RNA were reversely transcribed using Revert Aid First Strand cDNA synthesis kit (Thermo Fisher Scientific), according to the manufacturer's instructions. Resulting cDNA was diluted 1:10 in nuclease-free water before performing real time quantitative PCR.

To determine mRNA (messenger RNA) expression levels, qPCR was used. For this purpose, SYBR Green Master Mix (Applied Biosystems, Life Technologies) was mixed with specific cDNA and specific primers able to amplify the mRNA of interest. All qPCR reactions were run in technical triplicates on a 7500 Real-Time PCR System device (Applied Biosystems, Life Technologies). For all experiments, 18S ribosomal RNA expression was used as an endogenous control. Results were analyzed using the delta-delta Ct method. A total of at least 3 independent experiments was used for statistical analysis.

7.8 Flow cytometry

Cells were harvested and washed three times with FACS buffer (PBS + 0.5% BSA + 0.05% sodium azide). Afterwards, cells were incubated with directly conjugated APC

anti-human HLA-A, B, C antibody for 1h at 4°C. Next, cells were washed three times and DAPI was added to later distinguish between live and dead cells while measuring. Subsequently, cells were analyzed using a FacsCanto II (BD Biosciences) and results were analyzed using the FlowJo software. The general gating strategy is shown in Supplementary Fig. S1.

7.9 Cell cycle analysis

Cells were cultured and harvested after reaching 80% confluency. Afterwards, they were washed with ice-cold PBS. Next, cells were resuspended in PBS and 70% ethanol was added dropwise while vortexing for fixation. Samples were stored for fixation at 4°C over night. The next day, PBS was added and after centrifugation supernatant was removed. Next, samples were treated with 0.5 mg/ml RNase A (diluted in PBS) for 20 min at 37°C. Lastly, 40 µg/ml of propidium iodide (PI) were added and incubated for 30 min in the dark at RT. Samples were analyzed by flow cytometry using an LSR Fortessa HTS (BD Biosciences) and results were analyzed using the FlowJo software.

7.10 T cell cytotoxicity assay

10,000 cells/well were seeded on an xCELLigence E-Plate 96 PET (Agilent). The plate was incubated in an xCELLigence RTCA MP working station (ACEA Bioscience) located in an incubator. The working station was operated using the xCELLigence RTCA MP analyzer (ACEA Bioscience). 24h later, 100,000 MART-1-(melanoma antigen recognized by T cells 1) specific T cells were added to the cells. Killing was recorded by measuring the change in the impedance of the plates. After 36h, recording was stopped and data were analyzed using Prism 5.0 software (GraphPad). The optimal number of T cells used, was determined by titration of different amounts (0; 6,250; 12,500; 25,000; 50,000; and 100,000) of MART-1-specific T cells at the 0h, 24h, and 36h time points (Supplementary Fig. S2). Giovanni Mastrogiulio from the Joint Immunotherapeutics Laboratory at the DKFZ assisted in performing this experiment.

7.11 Microarray gene expression profiling

Total RNA samples from EV (empty vector) and SCG2 OE (overexpression) cells were processed by the Genomics and Proteomics Core Facility at the DKFZ by using the Clariom S human v1 r1 assay (Affymetrix). Data were then analyzed by Thomas Hielscher from the biostatistics division at DKFZ using the statistical software R 4.0 [159]. In short, he used

the Affymetrix CEL files, which at first were RMA normalized, and log2-transformed the expression values. Next, the empirical Bayes approach was used to identify differentially expressed probe sets/genes between groups [160]. This method is based on moderated t-statistics as implemented in the Bioconductor package limma [161]. The camera test was used for the gene set enrichment analysis [162]. For pathway analysis, KEGG, Reactome, and gene ontology data bases were used [163–165]. The Benjamini-Hochberg correction was employed for adjusting all p-values for multiple testing in order to control the false discovery rate (FDR). Microarray results were uploaded to the GEO database (GSE203179).

7.12 Bacterial transformation and plasmid isolation

For bacterial transformation and plasmid isolation, Stbl3 competent Escherichia coli (E.coli) bacteria were used. 100 µl of Stbl3 were thawn on ice and about 10 µl of the DNA of interest were added. The bacteria-DNA mix was then incubated 40 min on ice. After a heat shock of 3 min at 42°C, the mix was incubated for another 10 min on ice. Next, 500 µl SOC medium were added and the mix was incubated at 37°C for 1h under constant shaking. For plating, 50 µl of the suspension were plated onto agarose plates containing an antibiotic for selection. These plates were incubated over night at 37°C in a bacterial incubator. The next day, 5-10 clones were picked and grown in LB-medium containing the antibiotic for selection over night at 37°C under constant shaking. The following day, DNA was isolated using the Qiaprep Spin Miniprep Kit (Qiagen) according to the manufacturer's instructions. To ensure that the isolated plasmid was the plasmid of interest a restriction digest was performed and for further proof, the plasmid DNA sequence sequenced (LGC Genomics). The bacteria carrying the plasmid of interest were further cultivated in 200 ml LB-medium supplemented with the antibiotic for selection at 37°C over night. Using the Endofree Plasmid Maxi Kit (Invitrogen), plasmid DNA was isolated the next day. The Kit was used according to the manufacturer's instructions. Lastly, the concentration and quality of the isolated plasmid DNA were determined using the Nanodrop ND-1000.

7.13 Dataset analysis

Correlation of SCG2 with HLA-A, HLA-B, and HLA-C mRNA expression levels in melanoma from the GSE database (GSE7553) were analyzed [166]. The same expression data from GSE database (GSE7553) were used for a comparison of SCG2 expression levels

in normal skin, primary melanomas, and melanoma metastases. The mRNA expression data were provided by R2 Genomics analysis and visualization platform (http://hgserver1.amc.nl) accessed on 11th February 2022. Data for patient survival analysis were obtained from DFCI, Nature Medicine 2019 (www.cbioportal.org) accessed 31st August 2021 [167].

7.14 Statistical analysis

Statistical analyses were performed using Prism 5.0 software (GraphPad). Experiments were performed at least in triplicates if not mentioned otherwise. A two-tailed student's t test was performed to compare two groups and a one-way ANOVA (analysis of variance) to compare multiple conditions and data sets. Furthermore, Spearman's correlation was employed to define the connection of two paramenters and the Kaplan-Meier method was applied for survival analysis. All data are represented as mean ± SEM and statistical significance is indicated with the p-value scale (*$p<0.05$; **$p<0.01$; ***$p<0.001$; "ns" (not significant) $p>0.5$).

8 Results

8.1 High intratumoral SCG2 expression negatively affects the survival of melanoma patients

In order to investigate, if SCG2 expression levels have an influence on patient survival I analyzed data obtained from DFCI, Nature Medicine 2019 (n=121; Fig. 4A) [167]. Patients with high intratumoral SCG2 expression (Log2 SCG2≥1) showed a tendency towards lower survival rate (p=0.0531) than patients with lower SCG2 expression (Log2 SCG2<1). Next, I compared SCG2 expression levels in normal skin, primary melanomas, and melanoma metastases using data from a GSE database (GSE7553) [166]. I found significantly higher SCG2 expression levels in primary melanomas and melanoma metastases compared to normal skin (Fig. 4B). In addition to the data I obtained from databases, I analyzed SCG2 expression in a cohort of late-stage melanoma patient specimens with immunohistochemistry (IHC). The results were consistent with the survival data obtained from DFCI, Nature Medicine 2019 [167], showing that patients with high intratumoral SCG2 levels (SCG2 overall score>3) have a lower survival rate (p=0.0529) than patients with low SCG2 levels (SCG2 overall score≤3; Fig. 4C). Moreover, patients with high intratumoral SCG2 levels showed a significantly higher short-term survival (<12 months), whereas patients with low SCG2 levels showed higher long-term survival (≥12 months; Fig. 4D). Additionally, within this cohort of clinical specimens the comparison of SCG2 IHC overall score for nevi, primary melanomas, and melanoma metastases revealed higher SCG2 expression levels in primary melanomas and a tendency for a higher expression in melanoma metastases (Fig. 4E). This finding verified the results from the GSE database in Fig. 4B. Taken together, these data indicate a role of SCG2 in primary melanoma and melanoma metastases and therefore suggest that SCG2 might be a promising prognostic factor in melanoma.

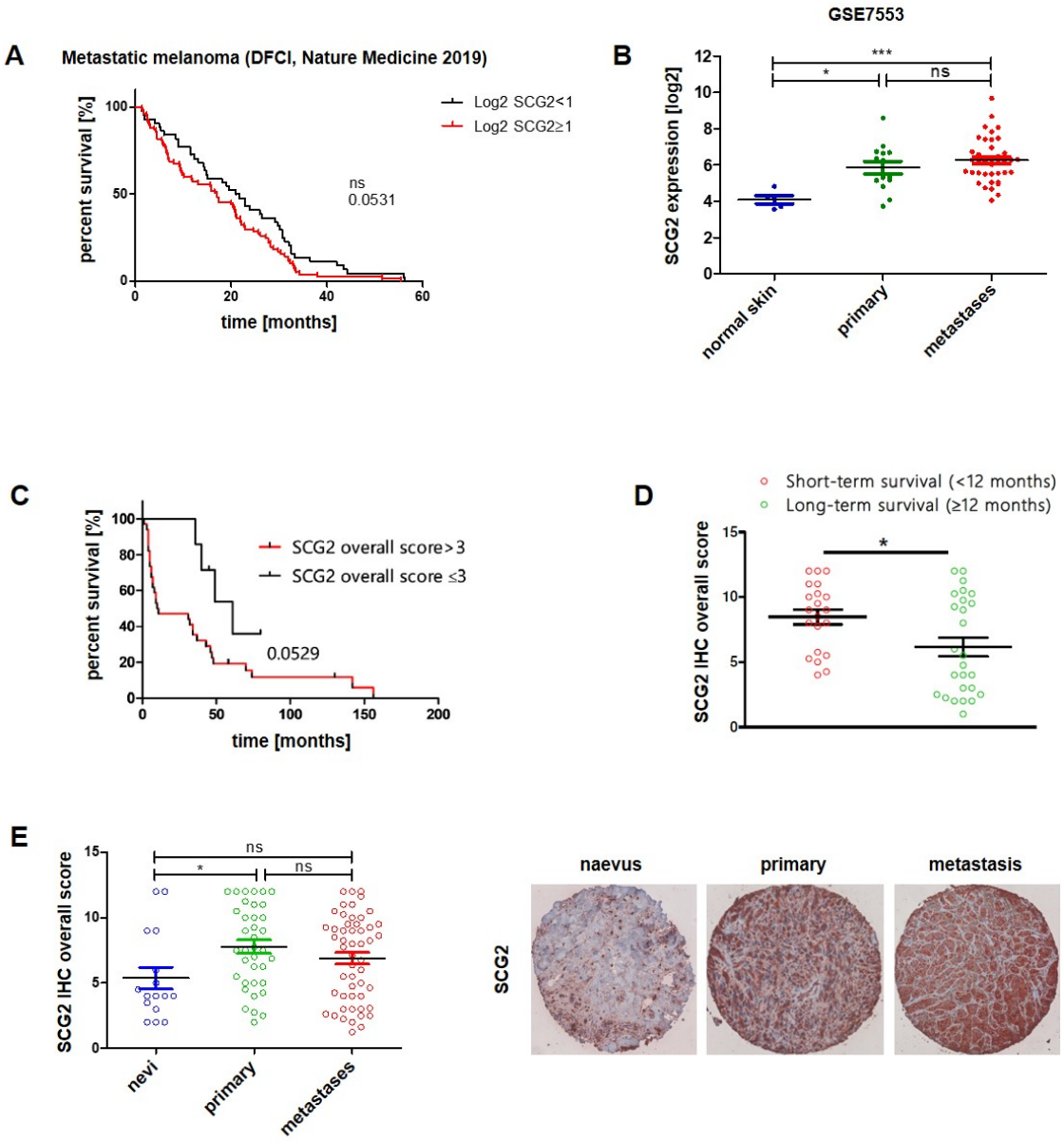

Fig. 4: High intratumoral SCG2 expression negatively affects the survival of melanoma patients.
A Kaplan-Meier curve comparing the overall survival of patients with metastatic melanoma (n=121) with low intratumoral SCG2 expression (Log2 SCG2<1) and those with high intratumoral SCG2 expression (Log2 SCG2≥1; p=0.0531). Expression data were obtained from DFCI, Nature Medicine 2019 [167]. **B** SCG2 expression levels (as log2) in normal skin (blue; n=5), primary melanomas (green; n=14), and melanoma metastases (red; n=40). Data were obtained from a GSE database (GSE7553) [166]. **C** Kaplan-Meier survival analysis comparing patients with melanoma metastases with a high SCG2 immunohistochemistry (IHC) overall score (SCG2 overall score>3) to patients with a lower SCG2 IHC overall score (SCG2 overall score≤3; p=0.0529). **D** Comparison of SCG2 IHC overall score of short-term (<12 months) and long-term (≥12 months) surviving patients with melanoma metastases. **E** IHC staining of SCG2 in patient samples from nevi (blue; n=16), primary melanomas (green; n=37), and melanoma metastases (red; n=52). *p<0.05; ***p<0.001; "ns" refers to p>0.5. Parts of this figure have already been published in Federico, Steinfass et al., *Mol Ther Oncolytics* [156].

8.2 SCG2 OE does not affect melanoma cell proliferation

To investigate the effect of SCG2 overexpression (OE) on melanoma cells, I used lentiviral transduction to generate SCG2 OE WM266-4 and C32 melanoma cells. As a control I used the empty vector (EV). The OE was validated on mRNA and protein level by real-time qPCR and western blot analysis, respectively (Fig. 5A). In WM266-4 melanoma cells an almost 200-fold and in C32 melanoma cells an almost 1500-fold increase of *SCG2* mRNA was detected after OE compared to EV. 18S was used as an endogenous control. Densitometric analysis of the western blot revealed a 6.9-fold and 4-fold increase of SCG2 after OE compared to EV in WM266-4 and C32 melanoma cells, respectively. GAPDH was used as a loading control.

Previous studies indicated that SCG2 might be a downstream target of the histone methyltransferase SETDB1 and SETDB1 OE has been associated with a more proliferative phenotype of melanoma [156, 168]. For this reason, I wanted to determine if this increased proliferative effect also appears upon SCG2 OE. I performed cell cycle analysis using PI staining to compare WM266-4 and C32 EV and SCG2 OE melanoma cells (Fig. 5B). However, the results did not show any differences in the cell cycle phases between EV and SCG2 OE, in both, WM266-4 and C32 melanoma cells, demonstrating that SCG2 OE did not alter the proliferation of melanoma cells.

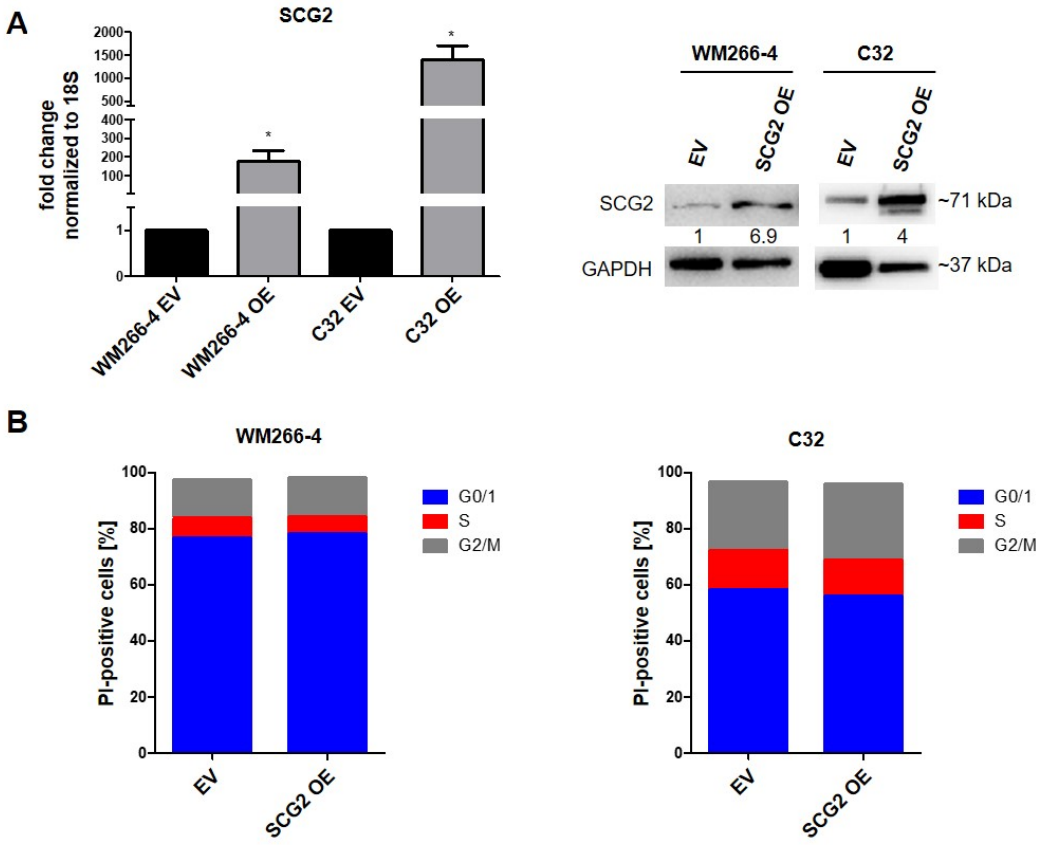

Fig. 5: SCG2 OE does not affect melanoma cell proliferation.
A Validation of SCG2 OE in WM266-4 and C32 melanoma cells on RNA (left) and protein (right) level. **B** Comparison of the cell cycle phases between WM266-4 (left) and C32 (right) EV and SCG2 OE melanoma cells with the help of PI (propidium iodide) staining followed by flow cytometric analysis. *$p<0.05$.

8.3 SCG2 OE influences the expression of several components of the APM

For an overview of the possible pathways affected by SCG2 OE, microarray analysis was performed and the KEGG, Gene Ontology, and Reactome databases were used for pathway prediction. The data showed that MHC class I antigen presentation might be influenced upon SCG2 OE (supplementary tables 1-6). To verify this finding, I analyzed the mRNA and protein expression of the endoplasmic reticulum markers calreticulin (CALR) and calnexin (CANX) after SCG2 OE (Fig. 6A and C). Together with tapasin (TAPBP), these proteins operate as chaperones in the MHC class I complex assembly [72,90]. I also determined the mRNA and protein expression of several other members of the APM after

SCG2 OE, which included TAP1, TAP2, B2M, and tapasin (Fig. 6B and C). CALR, CANX, TAP1, TAP2, B2M, and TAPBP showed decreased mRNA expression levels after SCG2 OE in WM266-4 and C32 melanoma cells (Fig. 6A and B). Western blot analysis of the corresponding proteins also confirmed a downregulation upon SCG2 OE in WM266-4 melanoma cells (Fig. 6C). However, western blot analysis of C32 only showed downregulation of calnexin, TAP2, TAP1, tapasin, and B2M, whereas calreticulin protein levels seemed to not be affected. GAPDH was used as a loading control.

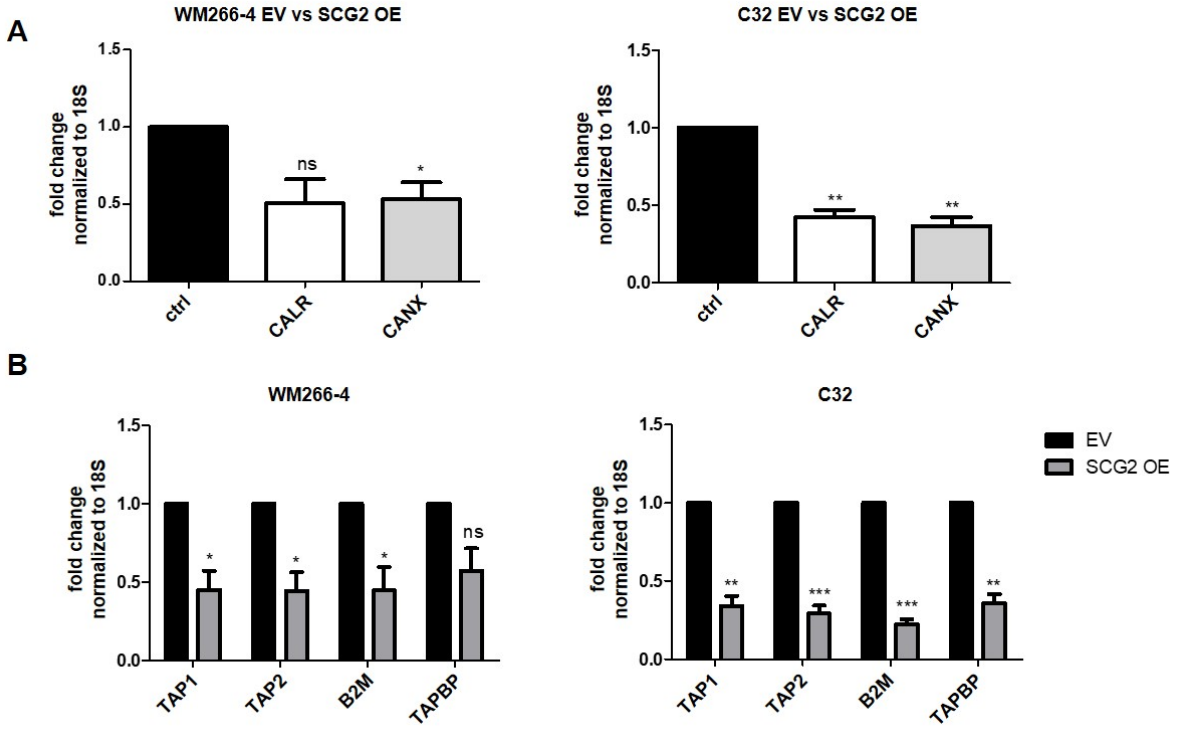

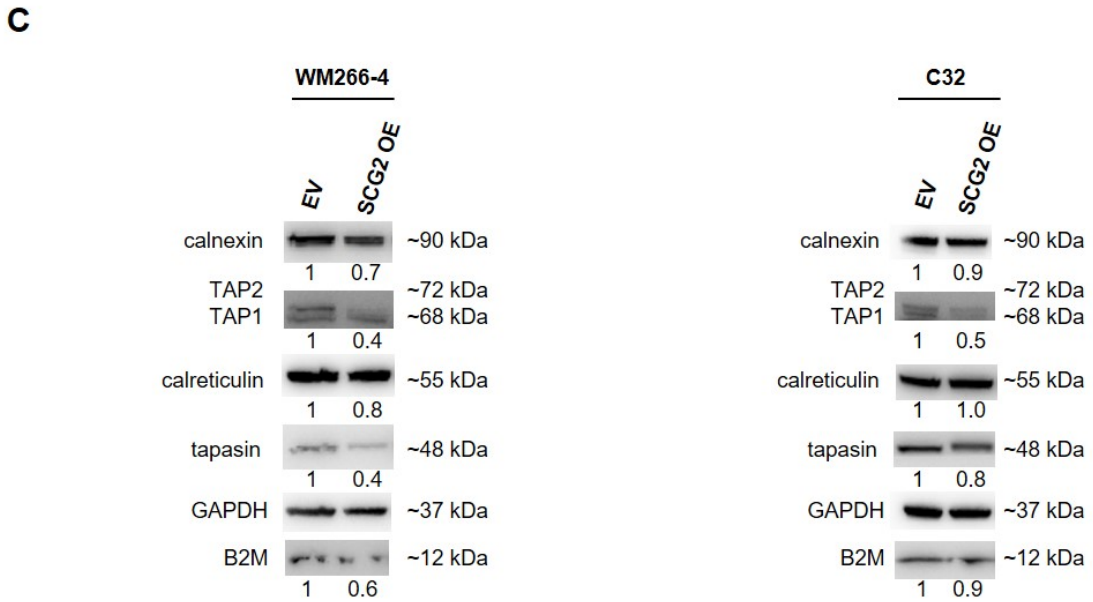

Fig. 6: SCG2 OE influences the expression of several components of the antigen presenting machinery (APM).
A Fold change of the mRNA expression levels of the ER markers and APM components calreticulin (CALR) and calnexin (CANX) upon SCG2 OE in WM266-4 (left) and C32 (right) melanoma cells. 18S was used as the endogenous control. **B** Fold change of the mRNA expression levels of the APM markers TAP1, TAP2, B2M, and tapasin (TAPBP) upon SCG2 OE in WM266-4 (left) and C32 (right) melanoma cells. 18S was used as the endogenous control. **C** Western blot analysis of the expression of the APM markers calnexin, TAP1, TAP2, calreticulin, tapasin, and B2M upon SCG2 OE in WM266-4 (left) and C32 (right) melanoma cells. GAPDH was used as the loading control. *$p<0.05$; **$p<0.01$; ***$p<0.001$; "ns" refers to $p>0.5$.

8.4 SCG2 expression levels negatively correlate with surface expression of MHC class I

The results presented so far indicate that the expression of several APM components decreased upon SCG2 OE (Fig. 6). Therefore, I wanted to investigate, if the expression of HLA-A, HLA-B, and HLA-C, which encode the heavy chain (HC) of the MHC class I complex in humans [68], was also affected by SCG2 OE. For this purpose, I analyzed expression data for SCG2, HLA-A, HLA-B, and HLA-C from melanoma patient samples (n=87) from a GSE database (GSE7553) and correlated them (Fig. 7A). The analysis showed a strong negative correlation between SCG2 and HLA-A ($p<0.001$), HLA-B ($p<0.01$), and HLA-C ($p<0.01$) expression. Plotting the expression levels of HLA-A, -B, and -C together in one graph and correlating them with SCG2 expression revealed that in most of the cases HLA-A, -B, and -C were expressed similarly in each individual patient sample, while showing some variation between patients. To gain further insight into the

effect of SCG2 on the MHC class I complex surface presentation, I compared the presence of surface HLA-ABC in WM266-4 and C32 EV and SCG2 OE cells using flow cytometry (Fig. 7B). Since the HC of the MHC class I complex is indispensable for the functionality, I concluded that the expression of HLA-A, HLA-B, and HLA-C is representative for the MHC class I complex itself. Flow cytometry results demonstrated a significant down-regulation of the mean fluorescence intensity (MFI) of HLA-ABC in WM266-4 and C32 SCG2 OE melanoma cells compared to the respective EV control cell line (Fig. 7B upper panel). Interestingly, the percentage of HLA-ABC$^+$ cells was not altered upon SCG2 OE (Fig. 7B lower panel). The general gating strategy used for flow cytometry analysis is depicted in Supplementary Fig. S1. Taken together, these data indicate a role of SCG2 in the process of MHC class I antigen surface presentation.

To examine, if the decrease in surface MHC class I also has a functional impact, I performed a T cell cytotoxicity assay using the xCELLigence RTCA impedance system. To observe the killing of EV and SCG2 OE melanoma cells over time, I used MART-1-specific T cells (added at time point 0h). MART-1 is a melanocyte-specific marker presented by MHC class I on the surface of melanoma cells. The optimal number of T cells for the experiment was determined by titrating different amounts of T cells at different time points (Supplementary Fig. S2). The neutralization of melanoma cells was plotted as the normalized cell index, which correlates with the cell number. This value results from the measured impedance created by the interaction of the WM266-4 and C32 melanoma cells with the gold biosensors in the plate. A decreasing normalized cell index represents cell killing, while an increase in the value refers to cell proliferation. The results revealed a significantly higher normalized cells index for both, WM266-4 and C32 SCG2 OE melanoma cells compared to the respective EV control cell line (Fig. 7C). Based on this finding, there is room to speculate that the decreased surface presentation of MHC class I on SCG2 OE melanoma cells reduced their sensitivity towards T cell-induced cytotoxicity.

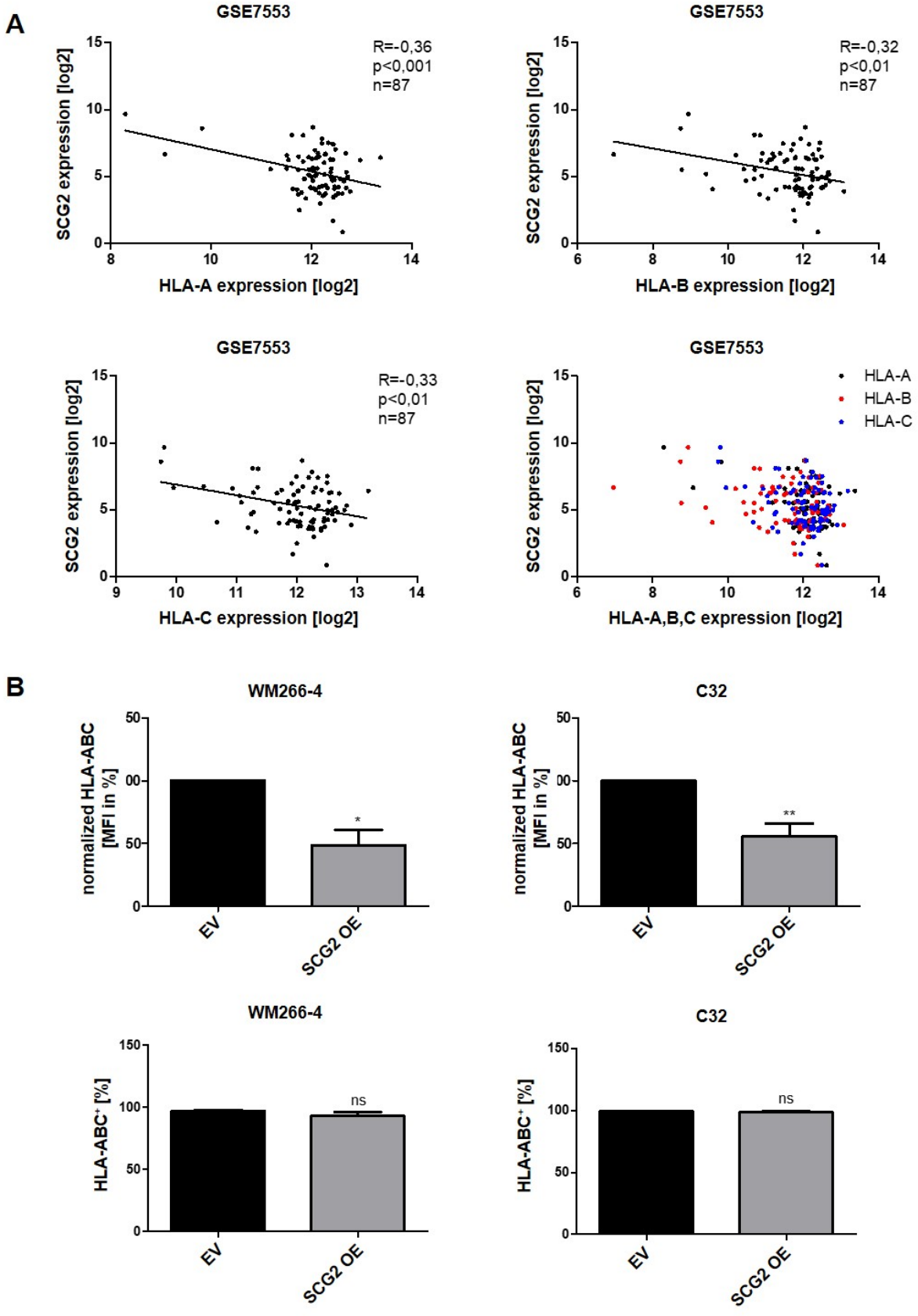
A
GSE7553
R=-0,36
p<0,001
n=87
SCG2 expression [log2]
HLA-A expression [log2]
GSE7553
R=-0,32
p<0,01
n=87
SCG2 expression [log2]
HLA-B expression [log2]
GSE7553
R=-0,33
p<0,01
n=87
SCG2 expression [log2]
HLA-C expression [log2]
GSE7553
HLA-A
HLA-B
HLA-C
SCG2 expression [log2]
HLA-A,B,C expression [log2]
B
WM266-4
normalized HLA-ABC [MFI in %]
*
EV
SCG2 OE
C32
normalized HLA-ABC [MFI in %]
**
EV
SCG2 OE
WM266-4
HLA-ABC+ [%]
ns
EV
SCG2 OE
C32
HLA-ABC+ [%]
ns
EV
SCG2 OE

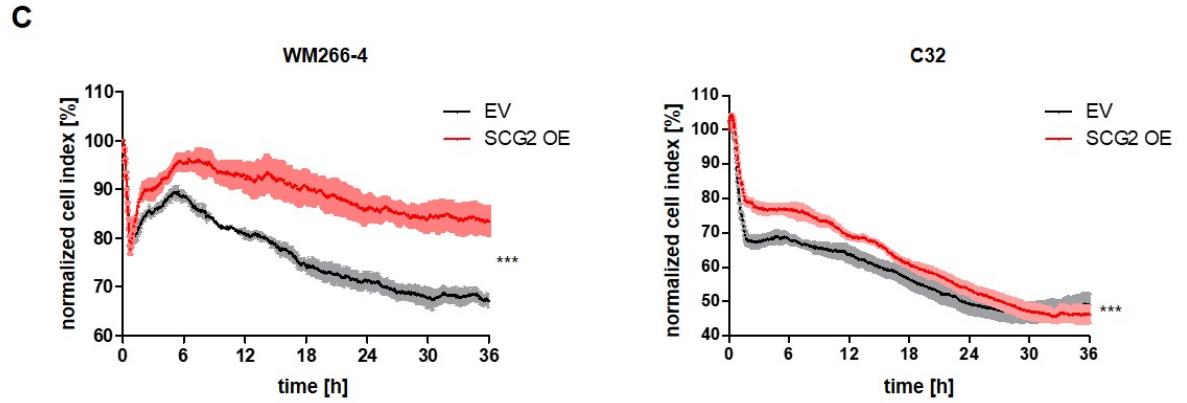

Fig. 7: SCG2 expression levels negatively correlate with surface MHC class I.
A Correlation of the expression data (log2) for SCG2 with HLA-A, HLA-B, and HLA-C from melanoma patients from GSE7553. Number of patient samples (n), correlation coefficient (R), and p-value (p) are indicated. **B** Top: comparison of the mean fluorescence intensity (MFI) of HLA-ABC between SCG2 OE and EV WM266-4 (left) and C32 (right) melanoma cells. The MFI positively correlates with the amount of HLA-ABC at the cell surface. Bottom: comparison of the number of HLA-ABC-positive (HLA-ABC$^+$) cells between SCG2 OE and EV WM266-4 (left) and C32 (right) melanoma cells. **C** xCELLigence RTCA impedance assay used to perform a T cell cytotoxicity assay with MART-1-specific T cells. Comparison of the normalized cell indices as a measure of the cell number between EV and SCG2 OE WM266-4 (left) and C32 (right) melanoma cells over time. The normalized cell index was determined by the impedance measured through the interaction of the cells with the gold biosensors. A decreasing normalized cell index indicates the neutralization of melanoma cells by cytotoxic T cells. *p<0.05; **p<0.01; ***p<0.001; "ns" refers to p>0.5.

8.5 SCG2-induced MHC class I downregulation can be partially restored by IFNγ

My results demonstrate that SCG2 OE led to a downregulation of several APM components resulting in a decrease of surface HLA-ABC, more specifically a decrease of surface MHC class I. It is already known that the expression of APM components and therefore the surface presentation of MHC class I can be stimulated through the IFNγ-induced activation of the Stat1 pathway [101,116]. Therefore, I investigated the effect of IFNγ on the surface HLA-ABC levels in SCG2 OE WM266-4 and C32 melanoma cells. I already showed that SCG2 OE resulted in a reduction of the HLA-ABC MFI of WM266-4 and C32 melanoma cells (Fig. 7B). Interestingly, after IFNγ treatment (10 ng/ml, 48h) of WM266-4 and C32 melanoma cells I could detect an increase of the MFI of HLA-ABC as well as no statistical difference between EV and SCG2 OE cells (Fig. 8A, upper panel). The percentage of HLA-ABC$^+$ WM266-4 and C32 melanoma cells did not change when comparing EV and SCG2 OE cells (Fig. 8A, lower panel). However, the percentage of HLA-ABC$^+$ cells was significantly higher for IFNγ-treated WM266-4 EV and SCG2 OE

cells compared to their untreated counterparts. This effect was not observable for C32 melanoma cells.

In order to verify the IFNγ-induced activation of the Stat1 pathway, I examined mRNA and protein expression levels of Stat1 (Fig. 8B and D). I observed a significant down-regulation of *STAT1* mRNA expression upon SCG2 OE in WM266-4 and C32 melanoma cells (Fig. 8B). The *STAT1* mRNA expression levels tendentially increased in both of the EV and SCG2 OE cell lines upon IFNγ treatment. When treated with IFNγ, WM266-4 SCG2 OE melanoma cells even showed a tendency for lower levels of *STAT1* mRNA expression compared to WM266-4 EV melanoma cells. Western blot analysis of total Stat1 and phospho-Stat1 (pStat1) protein levels in EV and SCG2 OE cells confirmed the mRNA expression data (Fig. 8D). Protein levels of total Stat1 and pStat1 increased after IFNγ treatment of WM266-4 and C32 EV and SCG2 OE melanoma cells compared to the untreated cells. When comparing the untreated cells, I observed a decrease of total Stat1 and pStat1 protein levels in the WM266-4 and C32 SCG2 OE cells.

Additionally, I examined the mRNA and protein expression levels of SCG2 in the untreated and IFNγ-treated WM266-4 and C32 EV and SCG2 OE melanoma cells (Fig. 8C and D). SCG2 mRNA expression levels did not change after IFNγ treatment (Fig. 8C). Interestingly, western blot analysis revealed a decrease in SCG2 protein levels in IFNγ-treated WM266-4 and C32 EV cells (Fig. 8D). SCG2 protein levels did not differ between untreated and treated WM266-4 and C32 SCG2 OE cells.

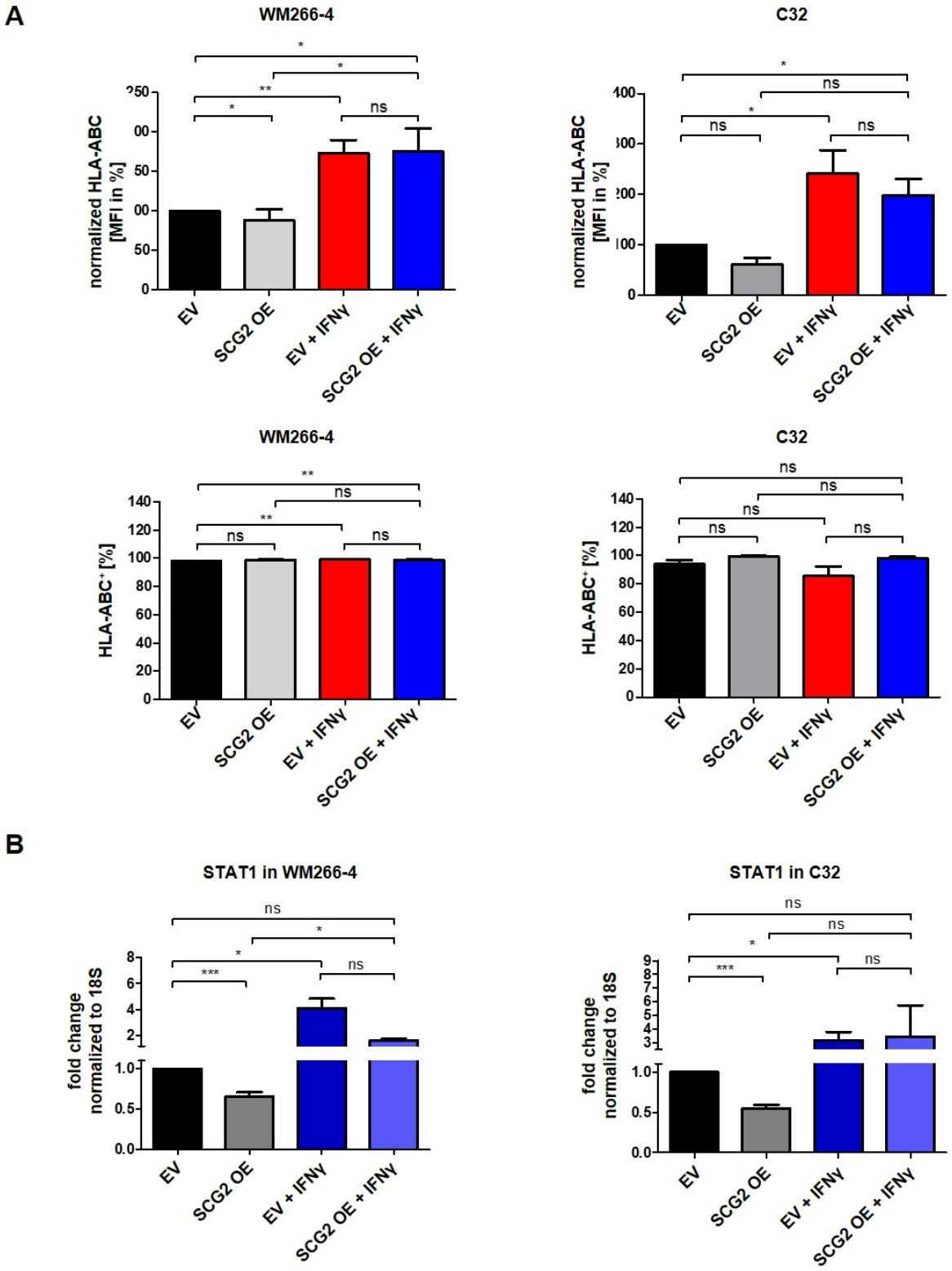
A
WM266-4
C32
normalized HLA-ABC [MFI in %]
HLA-ABC+ [%]
EV
SCG2 OE
EV + IFNγ
SCG2 OE + IFNγ
B
STAT1 in WM266-4
STAT1 in C32
fold change normalized to 18S
ns
*
**
***

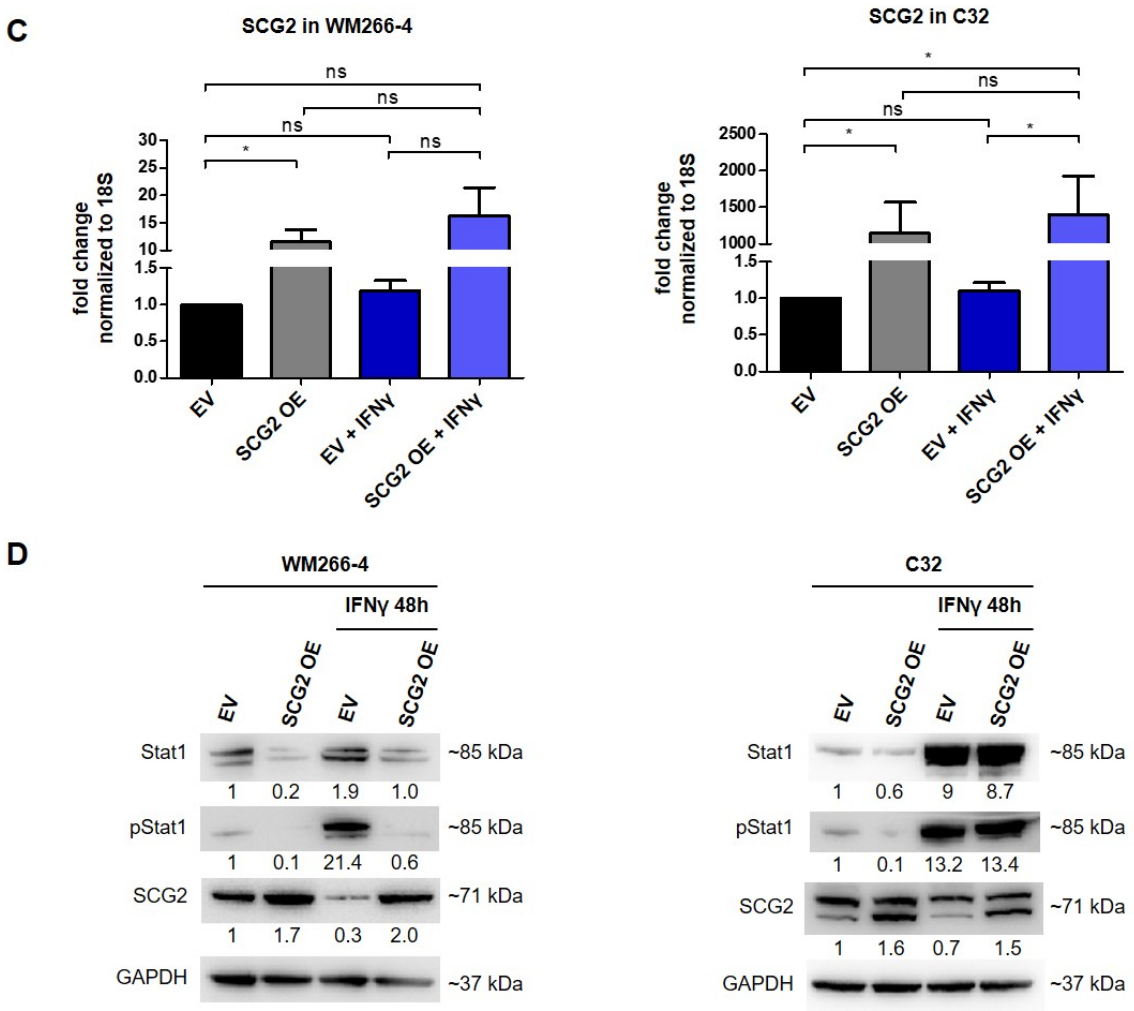

Fig. 8: SCG2-induced MHC class I downregulation can be partially restored by IFNγ. **A** Top: comparison of the MFI of HLA-ABC before and after IFNγ treatment (10 ng/ml, 48h) of WM266-4 (left) and C32 (right) EV and SCG2 OE melanoma cells. Bottom: comparison of the number of HLA-ABC$^+$ WM266-4 (left) and C32 (right) EV and SCG2 OE melanoma cells before and after IFNγ treatment. **B** Fold change of Stat1 mRNA expression levels in WM266-4 (left) and C32 (right) EV and SCG2 OE melanoma cells before and after IFNγ treatment. 18S was used as the endogenous control. **C** Fold change of SCG2 mRNA expression levels in WM266-4 (left) and C32 (right) EV and SCG2 OE melanoma cells before and after IFNγ treatment. 18S was used as the endogenous control. **D** Western blot analysis of total Stat1, phosphorylated Stat1 (pStat1), and SCG2 in WM266-4 (left) and C32 (right) EV and SCG2 OE melanoma cells before and after IFNγ treatment. GAPDH was used as the loading control. *p<0.05; **p<0.01; ***p<0.001; "ns" refers to p>0.5.

8.6 SCG2-induced downregulation of APM components can be partially restored by IFNγ

Since I observed an increase of the MFI of surface HLA-ABC upon IFNγ treatment, I also examined the changes in the expression of several APM components, including TAP1, TAP2, B2M, and TAPBP after IFNγ treatment. The results showed an upregulation of the mRNA expression of *TAP1*, *TAP2*, and *B2M* after IFNγ treatment in WM266-4 and C32 EV and SCG2 OE melanoma cells where SCG2 OE cells reached mRNA expression levels of the control cells (Fig. 9A). Interestingly, the *TAP1* mRNA expression of SCG2 OE and IFNγ-treated WM266-4 melanoma cells remained lower than in the control group. Moreover, IFNγ treatment did not increase *TAPBP* mRNA expression levels of SCG2 OE WM266-4 and C32 melanoma cells.

I also validated mRNA expression results for TAP1, TAP2, B2M, and TAPBP on the protein level using western blot analysis (Fig. 9B). The results confirmed the upregulation of TAP1, TAP2, and B2M after IFNγ treatment in C32 SCG2 OE melanoma cells. Upon IFNγ treatment, WM266-4 cells showed an increase of tapasin and B2M protein levels in SCG2 OE cells and tapasin protein levels remained constant in C32 SCG2 OE cells compared to untreated SCG2 OE cells. Comparing the results from the untreated cells, I observed lower protein levels of TAP2, TAP1, tapasin, and B2M in WM266-4 and C32 SCG2 OE cells compared to EV cells.

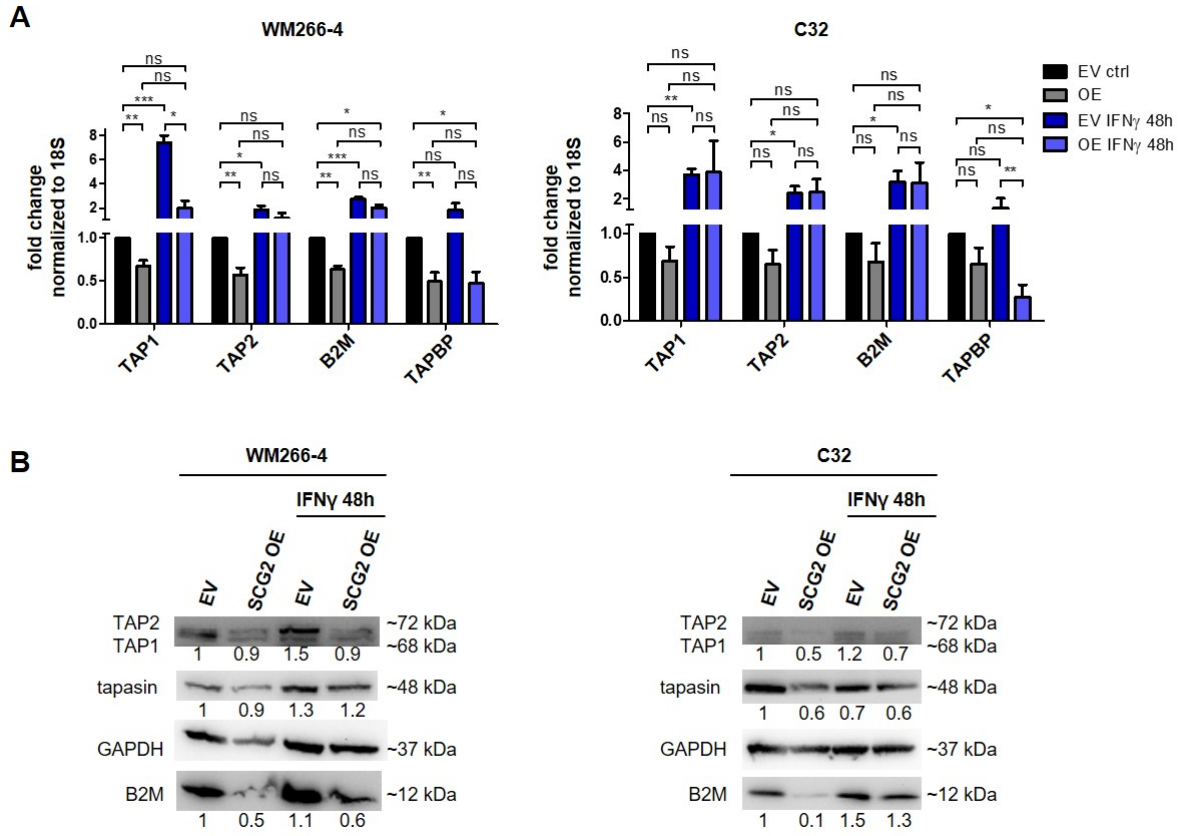

Fig. 9: SCG2-induced downregulation of several APM components can be partially restored by IFNγ.
A Fold change of *TAP1*, *TAP2*, *B2M*, and *TAPBP* mRNA expression levels in WM266-4 (left) and C32 (right) EV and SCG2 OE melanoma cells before and after IFNγ treatment. 18S was used as the endogenous control. **B** Western blot analysis of TAP1, TAP2, tapasin, and B2M expression in WM266-4 (left) and C32 (right) EV and SCG2 OE melanoma cells before and after IFNγ treatment. GAPDH was used as the loading control. *p<0.05; **p<0.01; ***p<0.001; "ns" refers to p>0.5.

8.7 SCG2 OE melanoma cells are more resistant towards cytotoxic T cell-induced killing

To investigate the functional effect of the upregulation of APM component expression and surface presentation of HLA-ABC after IFNγ treatment on WM266-4 and C32 melanoma cells, I performed another xCELLigence RTCA impedance assay with MART-1-specific T cells (Fig. 10). For both melanoma cell lines the results were similar. The normalized cell index was significantly lower upon IFNγ treatment of EV and SCG2 OE cells compared to untreated EV and SCG2 OE cells (EV vs. EV IFNγ and SCG2 OE vs. SCG2 OE IFNγ) indicating faster killing of these cells. The comparison of IFNγ-treated EV with IFNγ-treated SCG2 OE cells (EV IFNγ vs. SCG2 OE IFNγ) showed a higher normalized cell index for SCG2 OE cells. Comparing the untreated cells (EV vs. SCG2 OE), the results were consistent with the results shown in Fig. 7C. There I already showed that SCG2 OE melanoma cells were less sensitive towards T cell-induced cytotoxicity, which was caused by the decrease of surface MHC class I.

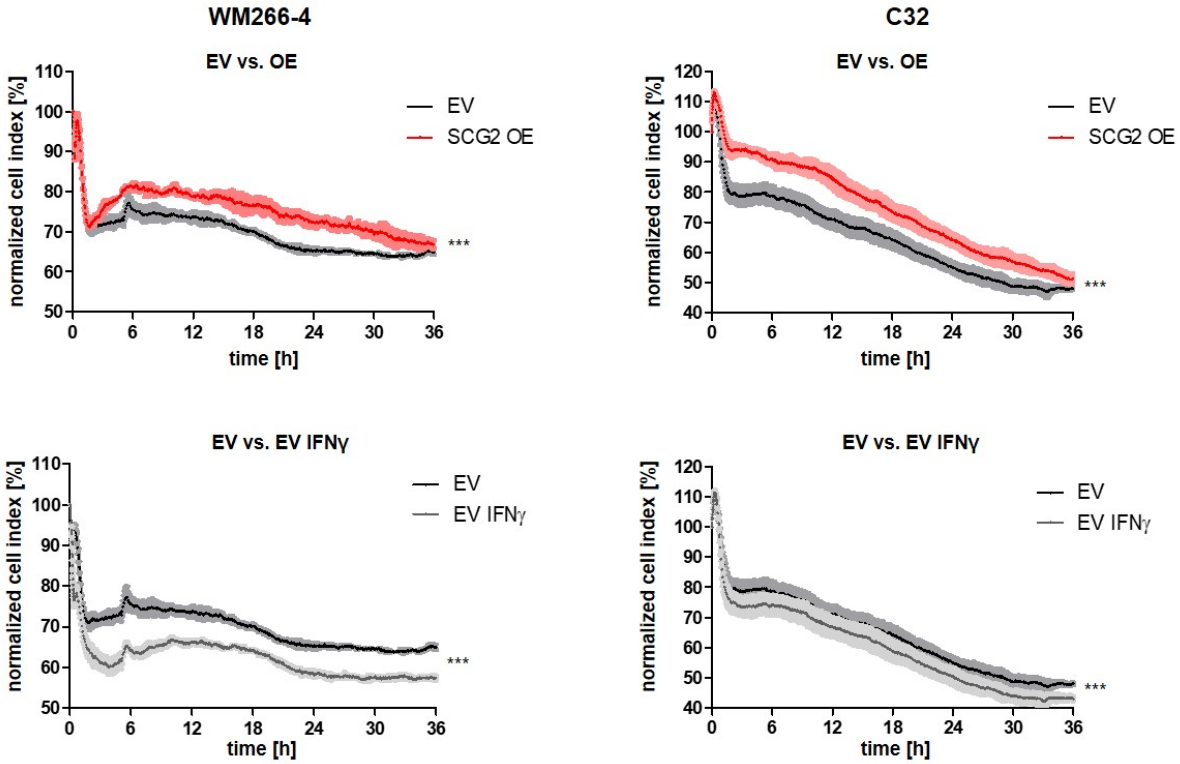

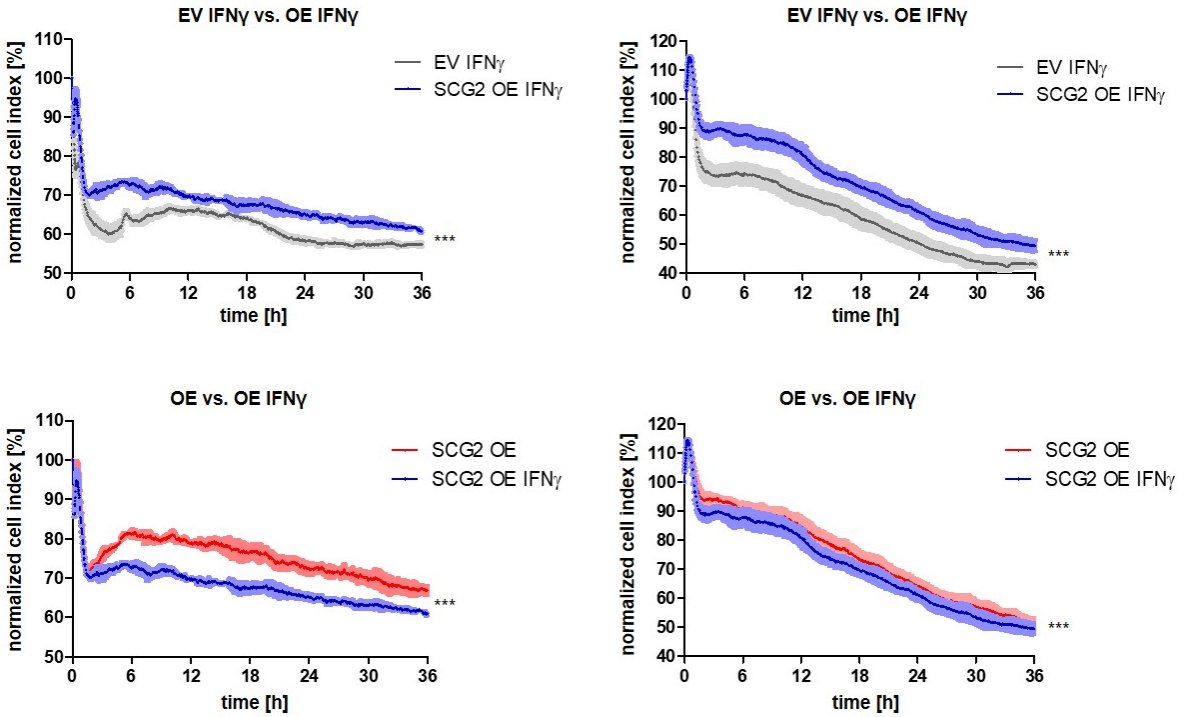

Fig. 10: SCG2 OE melanoma cells are more resistant towards cytotoxic T cell-induced killing.
xCELLigence RTCA impedance assay was used to perform a T cell cytotoxicity assay with MART-1-specific T cells. Comparison of the normalized cell indices as a measure of the cell number between WM266-4 (left) and C32 (right) EV and SCG2 OE melanoma cells over time as well as before and after IFNγ treatment. ***$p<0.001$.

8.8 SCG2 knockdown (KD) has an opposite effect than that of SCG2 OE

In order to investigate the effect of SCG2 knockdown (KD) on melanoma cells, I generated C32 and HT144 SCG2 KD melanoma cells using *SCG2*-specific shRNA. Non-targeting (NT) shRNA was used as the control group. I validated *SCG2* KD on the mRNA and protein level (Fig. 11A). The KD cells showed almost 70-fold less *SCG2* mRNA levels compared to the NT control and western blot analysis demonstrated a 0.2 and 0.5-fold decrease of SCG2 in C32 and HT144 SCG2 KD cells, respectively.

I also determined the mRNA and protein expression levels of the APM components calreticulin, calnexin, TAP1, TAP2, B2M, and tapasin (Fig. 11B-D). The mRNA expression levels of all APM components tested were significantly upregulated after SCG2 KD in HT144 (Fig. 11B-C). In C32 SCG2 KD cells, these APM components showed a tendency towards upregulation with the exception of tapasin. Western blot analysis of C32 and HT144 SCG2 KD melanoma cells revealed an increase of calnexin, TAP1, TAP2, and calreticulin protein levels (Fig. 11D). For HT144 also tapasin protein level was increased, whereas in C32 SCG2 KD melanoma cells the tapasin as well as the B2M protein level remained constant. The B2M protein level even slightly decreased in HT144 SCG2 KD cells.

Next, I investigated if this upregulation of several APM components upon SCG2 KD also led to an increase of MHC class I surface levels. My analysis indicated a significant increase of the MFI of HLA-ABC of C32 and HT144 melanoma cells (Fig. 11E). However, comparable to the situation upon SCG2 OE the percentage of HLA-ABC$^+$ cells remained unchanged.

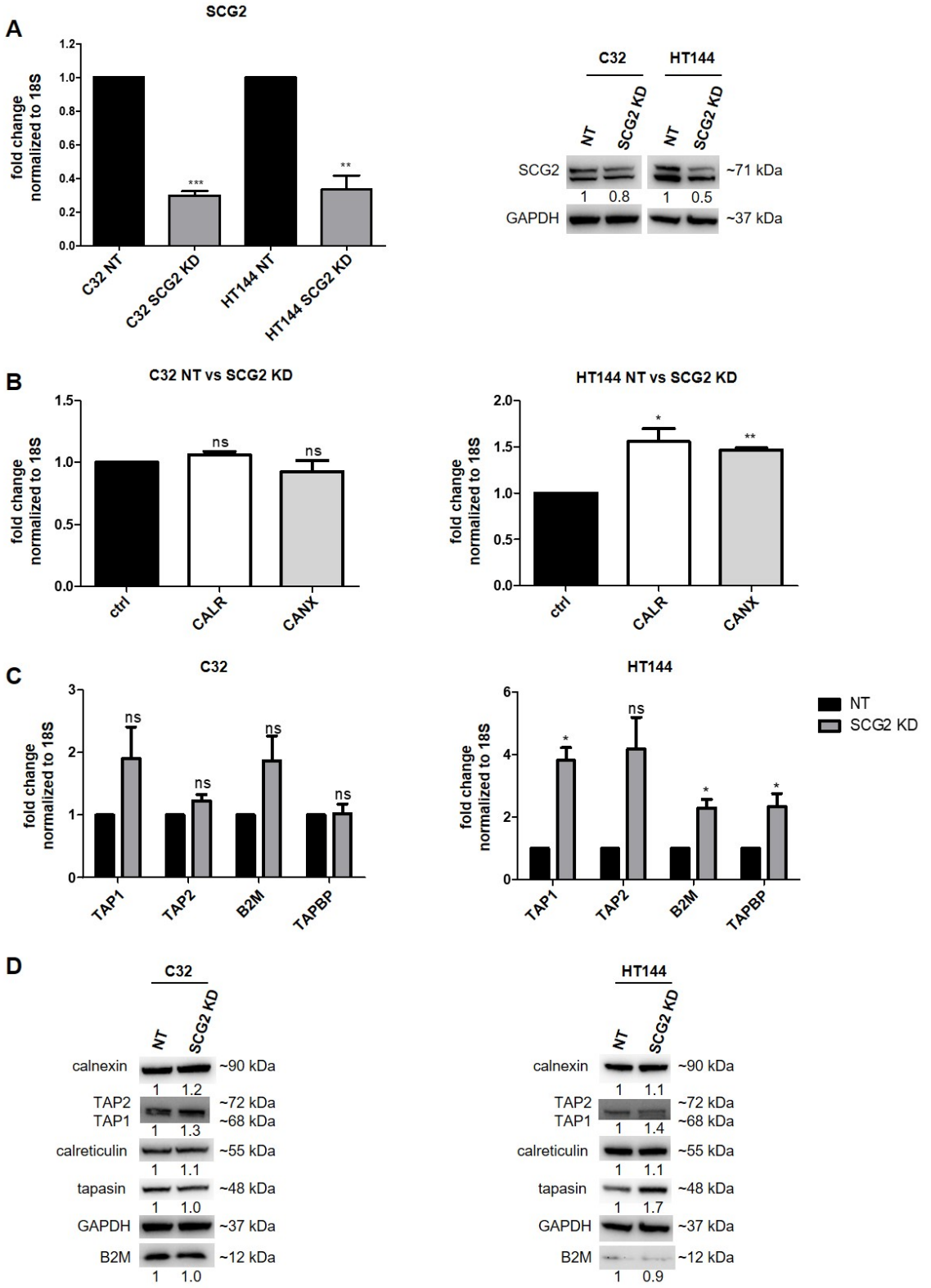
A
SCG2
fold change normalized to 18S
1.2
1.0
0.8
0.6
0.4
0.2
0.0
***
**
C32 NT
C32 SCG2 KD
HT144 NT
HT144 SCG2 KD
C32
HT144
NT
SCG2 KD
NT
SCG2 KD
SCG2
~71 kDa
1 0.8 1 0.5
GAPDH
~37 kDa
B
C32 NT vs SCG2 KD
fold change normalized to 18S
1.5
1.0
0.5
0.0
ns
ns
ctrl
CALR
CANX
HT144 NT vs SCG2 KD
fold change normalized to 18S
2.0
1.5
1.0
0.5
0.0
*
**
ctrl
CALR
CANX
C
C32
fold change normalized to 18S
3
2
1
0
ns
ns
ns
ns
TAP1
TAP2
B2M
TAPBP
HT144
fold change normalized to 18S
6
4
2
0
*
ns
*
*
TAP1
TAP2
B2M
TAPBP
NT
SCG2 KD
D
C32
NT
SCG2 KD
calnexin
~90 kDa
1 1.2
TAP2
TAP1
~72 kDa
~68 kDa
1 1.3
calreticulin
~55 kDa
1 1.1
tapasin
~48 kDa
1 1.0
GAPDH
~37 kDa
B2M
~12 kDa
1 1.0
HT144
NT
SCG2 KD
calnexin
~90 kDa
1 1.1
TAP2
TAP1
~72 kDa
~68 kDa
1 1.4
calreticulin
~55 kDa
1 1.1
tapasin
~48 kDa
1 1.7
GAPDH
~37 kDa
B2M
~12 kDa
1 0.9

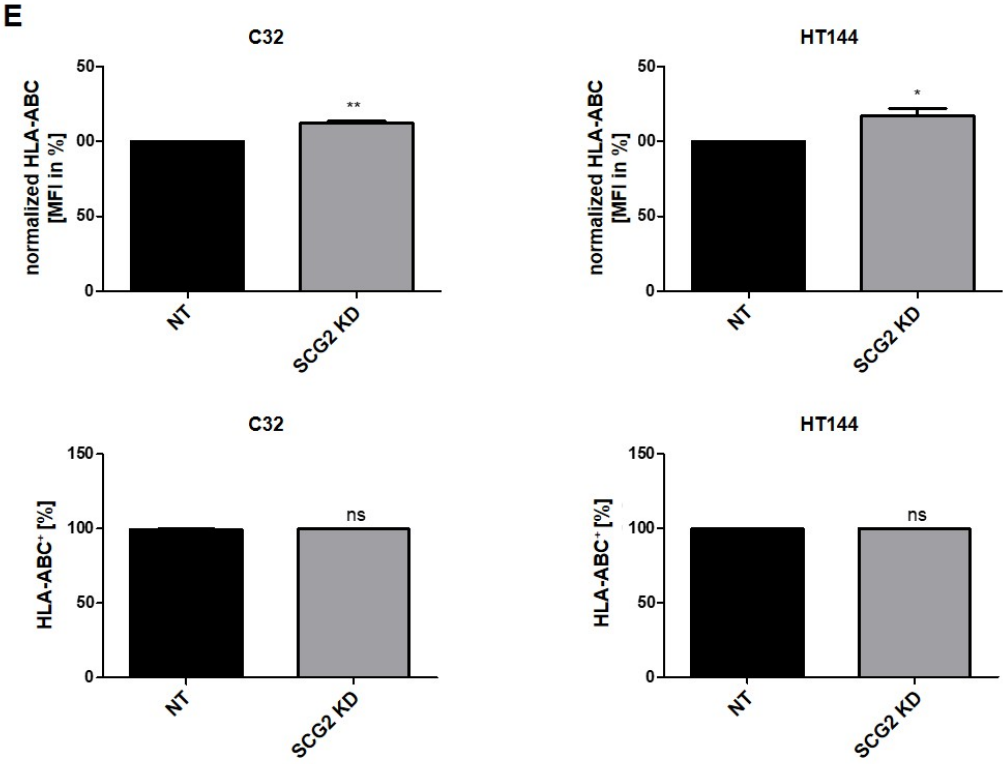

Fig. 11: SCG2 knockdown (KD) has an opposite effect than that of SCG2 OE.
A Validation of SCG2 knockdown (KD) in C32 and HT144 melanoma cells on the RNA (left) and protein (right) level. **B** Fold change of the mRNA expression of the ER markers and APM components calreticulin (CALR) and calnexin (CANX) upon SCG2 KD in C32 (left) and HT144 (right) melanoma cells. 18S was used as the endogenous control. **C** Fold change of mRNA expression of the APM markers TAP1, TAP2, B2M, and TAPBP upon SCG2 KD in C32 (left) and HT144 (right) melanoma cells. 18S was used as the endogenous control. **D** Western blot analysis of the expression of the APM markers calnexin, TAP1, TAP2, calreticulin, tapasin, and B2M after SCG2 KD in C32 (left) and HT144 (right) melanoma cells. GAPDH was used as the loading control. **E** Top: comparison of the MFI of HLA-ABC after SCG2 KD in C32 (left) and HT144 (right) melanoma cells. Bottom: comparison of the percentage of HLA-ABC$^+$ C32 (left) and HT144 (right) melanoma cells after SCG2 KD. *p<0.05; **p<0.01; ***p<0.001; "ns" refers to p>0.5.

9 Discussion

Melanoma is a very aggressive form of skin cancer that is often associated with poor prognosis for the patient [2]. Unfortunately, the development of resistances against existing therapies negatively influences therapy success. Therefore, it is important to gain further insights into the mechanisms of melanoma development, progression, and therapy resistance to develop novel treatment options and combinations. A recent study reported a potential contributing role of SCG2 to melanoma pathogenesis [156]. However, the exact role of SCG2 in melanoma is still unclear. Hence, elucidating the SCG2-driven mechanisms in melanoma became the major topic of my study.
In the present work, I could show that i) high SCG2 expression correlated with poor survival rates of melanoma patients; ii) SCG2 was highly expressed in primary melanomas and metastases; iii) SCG2 OE led to a downregulation of components of the APM; iv) as a consequence the amount of surface MHC class I was downregulated; v) SCG2 OE melanoma cells were more resistant towards cytotoxic T cell-induced killing; vi) IFNγ treatment partially restored APM expression and surface MHC class I presentation; vii) IFNγ treatment sensitized SCG2 OE melanoma cells towards cytotoxic T cell-induced killing; viii) SCG2 KD increased the expression of APM components and the surface presentation of MHC class I. Based on these results, there is reason to speculate that SCG2 affects immune evasion mechanisms in melanoma and therefore could be associated with resistance towards checkpoint blockade and adoptive immunotherapy.

9.1 SCG2 influences patient survival but not melanoma cell proliferation

To assess, if SCG2 plays a potential role in melanoma, I analyzed publicly available data sets from patients with metastatic melanoma. The results showed that patients with high intratumoral SCG2 expression had a survival disadvantage over patients with low intratumoral SCG2 expression (Fig. 4A). This result was confirmed by the analysis of a cohort of specimens from patients with metastatic melanoma, revealing a survival benefit of patients with low intratumoral SCG2 expression levels over patients with high intratumoral SCG2 expression levels (Fig. 4C and D) [156]. The coherence between SCG2 expression and patient survival also has been found in colorectal cancer patients [150, 151, 169]. Additionally, I analyzed SCG2 expression data from a GSE database and compared SCG2 expression in normal skin, primary melanoma tumors and metastases. The data revealed higher SCG2 expression in primary tumors and metastases compared

to normal skin (Fig. 4B). I confirmed these results by analyzing the same parameters in the cohort of melanoma patient specimens (Fig. 4E). Based on these results, there is reason to speculate that SCG2 plays a role in melanoma. To study the role of SCG2 in melanoma, I generated SCG2 OE and KD melanoma cell lines (Fig. 5A and 11A).
Studies on the role of the histone methyltransferase SETDB1 in melanoma showed that SETDB1 influences the proliferative behavior [168]. A follow up study indicated that SCG2 might be a potential downstream target of SETDB1 in melanoma [168]. For this reason, I wanted to investigate, if SCG2 alters the proliferative behavior of melanoma cells. Additionally, previous studies on colorectal cancer demonstrated that SCG2 contributes to the progression of colorectal cancer by influencing the proliferative behavior [136]. To examine, if SCG2 affects melanoma cell proliferation I determined the percentage of SCG2 OE melanoma cells in S-Phase. However, I did not detect any differences in proliferation between control and SCG2 OE melanoma cells (Fig. 5B). It rather seems like SCG2 influences melanoma aggressiveness, indicated by the survival disadvantage of patients with high intratumoral SCG2 expression, through different mechanisms and that its role differs between different cancer types.

9.2 SCG2 OE alters the expression of several APM components and thus influences MHC class I cell surface presentation

To determine the pathways that might be affected upon SCG2 OE I used microarray gene expression profiling. The analysis revealed that the gene expression of various members of the APM, including calreticulin, calnexin, TAP1, TAP2, B2M, and tapasin was reduced in WM266-4 and C32 melanoma cells after SCG2 OE (Fig. 6A and B). The APM is indispensable for the assembly of the MHC class I complex [72, 83, 84, 90, 92, 100]. The MHC class I complex presents antigens on the cell surface to $CD8^+$ T cells, which get activated and neutralize cancer cells upon recognition of specific antigens [68, 72]. However, since the presence of MHC class I is not essential for cell survival, cancer cells develop mechanisms to escape this immune control by targeting the APM components and subsequently affecting the function of the MHC class I complex. This does not only have consequences for the immune response but also for the outcome of immune therapy [101]. A recent study on patients with advanced melanoma reported that patients are unlikely to respond to anti-PD-1 monotherapy, if the amount of MHC class I on the tumor cell surface is low. Nevertheless, these patients still respond to anti-PD-1 and anti-CTLA-4 combination treatment [170, 171]. Due to the instability of the MHC class I molecules, any defect in a single APM component can result in the loss of MHC class I presenta-

tion [72]. My western blot analyses depicted in Fig. 6C confirmed the downregulated expression of calnexin, TAP1, TAP2, B2M, and tapasin in WM266-4 and C32 melanoma cells after SCG2 OE. It has been reported that defects in the APM components TAP1, TAP2, and tapasin as well as the total loss of MHC class I contribute to melanoma progression [72, 103–107, 111, 112]. My observation of reduced calnexin, TAP1, TAP2, B2M, and tapasin expression in WM266-4 and C32 melanoma cells upon SCG2 OE on the mRNA as well as on the protein level together with the results of other published studies led to the assumption, that surface MHC class I could also be downregulated. To pursue this hypothesis, I determined HLA-ABC cell surface levels. Since the HC of the MHC class I complex is encoded by the HLA-A, -B, and -C genes [68], cell surface levels of HLA-ABC correspond to MHC class I cell surface levels. I detected lower MHC class I cell surface levels after SCG2 OE and thus could confirm the hypothesis (Fig. 7B). I could further verify this finding by analyzing patient data from a GSE database. The data revealed a negative correlation between SCG2 and HLA-A, -B, and -C gene expression levels (Fig. 7A). Moreover, the expression levels of the three HLA proteins were similar in each individual patient. This indicates that in most melanoma patients of this study SCG2 exerts its immune-modulatory effects by influencing the expression of all three genes, HLA-A, -B, and -C, at the same time and therefore influencing MHC class I in general and not a specific isotype of MHC class I. However, when looking at the number of HLA-ABC^{+} cells, I could not detect any differences between SCG2 OE and EV control cells (Fig. 7B). In summary, these results indicate that the cells did not completely lose surface MHC class I since they still were HLA-ABC-positive, but that SCG2 OE reduced the density of MHC class I on the cell surface. In contrast, I observed opposite effects in SCG2 KD C32 and HT144 melanoma cells (Fig. 11). Here, I noticed an upregulation of calnexin, TAP1, TAP2, and calreticulin in both, C32 and HT144 SCG2 KD melanoma cells, and subsequently an upregulation of MHC class I at the cell surface. However, the percentage of MHC class I-positive C32 and HT144 melanoma cells did not change. In summary, these results indicate that the expression level of SCG2 influenced the amount of MHC class I on the cell surface. Interestingly, the decreased surface presentation of MHC class I after SCG2 OE reduced the sensitivity of the WM266-4 and C32 melanoma cells towards T cell-induced cytotoxicity, as I could show using a T cell cytotoxicity assay (Fig. 7C). Based on this result, there is reason to speculate that the SCG2-induced downregulation of cell surface MHC class I might be a potential mechanism of melanoma cells to evade immune detection. To address this theory, one could use a suitable mouse model using murine SCG2 OE cells and, for example, compare immunological markers

and the size of the control tumor with the SCG2 OE tumor.

9.3 IFNγ counteracts SCG2-induced downregulation of APM components and surface MHC class I levels

It has been shown that restoring MHC class I cell surface presentation to a normal level resensitizes melanoma cells towards cytotoxic T cells [113, 114]. The loss of MHC class I in several cancer entities, including esophageal squamous cell carcinoma, lung cancer, and melanoma, is associated with the resistance towards checkpoint blockade and adoptive immune therapy [170–177]. However, also defective IFNγ-signaling can affect the response to immune checkpoint blockade therapy in melanoma [115]. Additionally, it has been shown that upregulating IFNγ signaling early during therapy leads to an improved outcome of immune checkpoint blockade in melanoma [171, 178, 179]. Here, I demonstrated that the decrease of cell surface MHC class I upon SCG2 OE in WM266-4 and C32 melanoma cells could be counteracted by IFNγ treatment (Fig. 8A). This seemed to be the result of the IFNγ-induced activation of Stat1, which is known to upregulate the expression of MHC class I surface components [116]. In the SCG2 OE melanoma cells, a strong upregulation of *STAT1* mRNA levels and activated Stat1 was detected after IFNγ treatment (Fig. 8B and D). This resulted in an increased expression of the APM components TAP1, TAP2, tapasin, and B2M in those cells (Fig. 9). Subsequently, another T cell cytotoxicity assay showed that the restored MHC class I cell surface presentation led to a higher sensitivity of the SCG2 OE cells towards T cells (Fig. 10). A study with B16 melanoma cells also demonstrated that the downregulation of some APM components and the subsequent reduction of MHC class I can be counteracted by IFNγ treatment [180]. Interestingly, the data I obtained showed that IFNγ-treated SCG2 OE cells were still less sensitive to T cell cytotoxicity compared to the IFNγ-treated EV cells, even though the flow cytometry results indicated that the density of cell surface MHC class I was partially restored after IFNγ treatment. Since it is known that cytotoxic T cells can induce apoptosis in the target cells to eliminate them, it is possible that SCG2 OE melanoma cells escape apoptosis by altering apoptotic pathways and thereby becoming resistant to T cell-induced killing despite the restoration of MHC I expression levels [181]. To test this theory, additional investigations of apoptotic pathways and apoptosis in response to T cell-induced killing could be performed. However, this theory could explain that, although MHC class I levels were restored, IFNγ-treated SCG2 OE melanoma cells were still more resistant towards cytotoxic T cells. Furthermore, in several studies the impact of the tumor secretome on the anti-tumor activity of immune cells was investigated. For example, it has been shown

that the secretion of HLA-G by tumor cells induces the upregulation of CTLA-4, PD-1, TIM-3, and CD95 on CD8 T cells and therefore influences their anti-tumor activity [182]. Additionally, in a recent study on colorectal cancer it has been found that SCG2 might play a role in regulating several tumor- and immune-related pathways and subsequently could be used as a prognostic marker [169]. However, further investigating the pathways affected by SCG2 and its possible influence on the tumor immune response are interesting topics for future studies.

10 Conclusion

In my study I discovered that SCG2 was highly expressed in primary melanomas and melanoma metastases and that high intratumoral SCG2 expression negatively influenced melanoma patient survival. Moreover, I showed that SCG2 influenced the assembly and cell surface presentation of the MHC class I complex. In detail, SCG2 OE led to a downregulation of several components of the APM and therefore resulted in lower cell surface levels of MHC class I accompanied by a reduced sensitivity of the melanoma cells towards T cell-induced cytotoxicity (Fig. 12). However, the downregulation of both, some of the APM components and cell surface MHC class I, could be partially restored by IFNγ treatment. Interestingly, the IFNγ-treated SCG2 OE cells were still more resistant towards cytotoxic T cells. Hence, I concluded that the Stat1-pathway was involved in the SCG2-driven effects on the MHC class I complex in melanoma. In summary, my results could contribute to the understanding of the role of SCG2 in melanoma immune evasion. Thus, SCG2 could function as a valuable prognostic factor concerning the success of checkpoint blockade and adoptive immunotherapy. Furthermore, investigations concentrating on the mechanisms and pathways involved in the SCG2-induced alteration of MHC class I complex surface presentation could contribute to the establishment of possible novel melanoma treatment options.

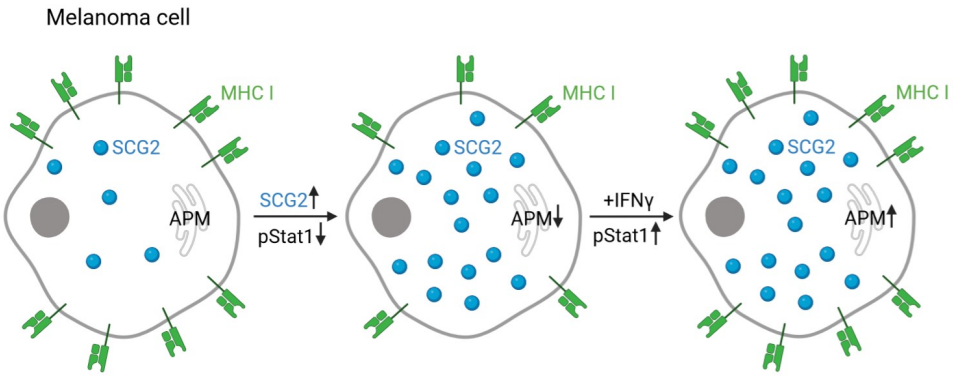

Fig. 12: Schematic summary of the SCG2 OE-induced effects on the APM and MHC class I in melanoma cells.
Melanoma cell with nucleus and ER represented in grey. SCG2 is intracellularly represented as blue circles and MHC class I complex is represented in green on the cell surface. Arrows facing up and down indicate up- and downregulation, respectively.

11 References

[1] N. H. Matthews, W. Q. Li, A. A. Qureshi, M. A. Weinstock, and E. Cho. Epidemiology of melanoma. *Cutaneous Melanoma: Etiology and Therapy*, 2017.

[2] A. Lideikaite, J. Mozuraitiene, and S. Letautiene. Analysis of prognostic factors for melanoma patients. *Acta Med Litu*, 24(1):25–34, 2017.

[3] WCRF International. Skin cancer statistics. *WCRF International*, 2021 (accessed July 23th, 2021). `https://www.wcrf.org/dietandcancer/skin-cancer-statistics/`.

[4] American Cancer Society. Cancer Facts and Figures 2018. *American Cancer Society*, 2018 (accessed January 29, 2019). `https://www.cancer.org/content/dam/cancer-org/research/cancer-facts-and-statistics/annual-cancer-facts-and-figures/2018/cancer-facts-and-figures-2018.pdf`.

[5] American Cancer Society. Risk Factors for Melanoma Skin Cancer. *American Cancer Society*, 2021 (accessed July 16th, 2021). `https://www.cancer.org/cancer/melanoma-skin-cancer/causes-risks-prevention/risk-factors.html`.

[6] K. Eddy and S. Chen. Overcoming immune evasion in melanoma. *Int J Mol Sci*, 21(23), 2020.

[7] A. Sandru, S. Voinea, E. Panaitescu, and A. Blidaru. Survival rates of patients with metastatic malignant melanoma. *J Med Life*, 7(4):572–6, 2014.

[8] W. E. Damsky, L. E. Rosenbaum, and M. Bosenberg. Decoding melanoma metastasis. *Cancers (Basel)*, 3(1):126–63, 2010.

[9] M. Tucci, A. Passarelli, F. Mannavola, C. Felici, L. S. Stucci, M. Cives, and F. Silvestris. Immune system evasion as hallmark of melanoma progression: The role of dendritic cells. *Front Oncol*, 9:1148, 2019.

[10] M. Brenner and V. J. Hearing. The protective role of melanin against UV damage in human skin. *Photochem Photobiol*, 84(3):539–49, 2008.

[11] J. Paluncic, Z. Kovacevic, P. J. Jansson, D. Kalinowski, A. M. Merlot, M. L. Huang, H. C. Lok, S. Sahni, D. J. Lane, and D. R. Richardson. Roads to melanoma: Key

pathways and emerging players in melanoma progression and oncogenic signaling. *Biochim Biophys Acta*, 1863(4):770–84, 2016.

[12] B. Bandarchi, C. A. Jabbari, A. Vedadi, and R. Navab. Molecular biology of normal melanocytes and melanoma cells. *J Clin Pathol*, 66(8):644–8, 2013.

[13] Y. Bermudez. Ultraviolet involvement in melanocyte transformation to melanoma. *Br J Dermatol*, 171(6):1289, 2014.

[14] A. H. Shain and B. C. Bastian. From melanocytes to melanomas. *Nat Rev Cancer*, 16(6):345–58, 2016.

[15] K. Eddy, R. Shah, and S. Chen. Decoding melanoma development and progression: Identification of therapeutic vulnerabilities. *Front Oncol*, 10:626129, 2020.

[16] C. Abildgaard and P. Guldberg. Molecular drivers of cellular metabolic reprogramming in melanoma. *Trends Mol Med*, 21(3):164–71, 2015.

[17] W. J. Mooi and D. S. Peeper. Oncogene-induced cell senescence–halting on the road to cancer. *N Engl J Med*, 355(10):1037–46, 2006.

[18] E. Shtivelman, M. Q. Davies, P. Hwu, J. Yang, M. Lotem, M. Oren, K. T. Flaherty, and D. E. Fisher. Pathways and therapeutic targets in melanoma. *Oncotarget*, 5(7):1701–52, 2014.

[19] R. M. Cymerman, Y. Shao, K. Wang, Y. Zhang, E. C. Murzaku, L. A. Penn, I. Osman, and D. Polsky. De novo vs nevus-associated melanomas: Differences in associations with prognostic indicators and survival. *J Natl Cancer Inst*, 108(10), 2016.

[20] M. H. Greene, Jr. Clark, W. H., M. A. Tucker, K. H. Kraemer, D. E. Elder, and M. C. Fraser. High risk of malignant melanoma in melanoma-prone families with dysplastic nevi. *Ann Intern Med*, 102(4):458–65, 1985.

[21] S. Mocellin and D. Nitti. Cutaneous melanoma in situ: translational evidence from a large population-based study. *Oncologist*, 16(6):896–903, 2011.

[22] J. Villanueva and M. Herlyn. Melanoma and the tumor microenvironment. *Curr Oncol Rep*, 10(5):439–46, 2008.

[23] S. L. Wong, M. B. Faries, E. B. Kennedy, S. S. Agarwala, T. J. Akhurst, C. Ariyan, C. M. Balch, B. S. Berman, A. Cochran, K. A. Delman, M. Gorman, J. M. Kirkwood, M. D. Moncrieff, J. S. Zager, and G. H. Lyman. Sentinel lymph node biopsy and management of regional lymph nodes in melanoma: American society of clinical oncology and society of surgical oncology clinical practice guideline update. *J Clin Oncol*, 36(4):399–413, 2018.

[24] F. Tas. Metastatic behavior in melanoma: timing, pattern, survival, and influencing factors. *J Oncol*, 2012:647684, 2012.

[25] B. Domingues, J. M. Lopes, P. Soares, and H. Populo. Melanoma treatment in review. *Immunotargets Ther*, 7:35–49, 2018.

[26] C. Esnault, D. Schrama, R. Houben, S. Guyetant, A. Desgranges, C. Martin, P. Berthon, M. C. Viaud-Massuard, A. Touze, T. Kervarrec, and M. Samimi. Antibody-Drug Conjugates as an Emerging Therapy in Oncodermatology. *Cancers (Basel)*, 14(3), 2022.

[27] M. Batus, S. Waheed, C. Ruby, L. Petersen, S. D. Bines, and H. L. Kaufman. Optimal management of metastatic melanoma: Current strategies and future directions. *Am J Clin Dermatol*, 14(3):179–94, 2013.

[28] S. J. O'Day, C. J. Kim, and D. S. Reintgen. Metastatic melanoma: Chemotherapy to biochemotherapy. *Cancer Control*, 9(1):31–8, 2002.

[29] M. A. Wilson and L. M. Schuchter. Chemotherapy for melanoma. *Cancer Treat Res*, 167:209–29, 2016.

[30] W. Shi. Radiation Therapy for Melanoma. Editors: W.H. Ward and J.M. Farma. *Cutaneous Melanoma: Etiology and Therapy*, Brisbane (AU), 2017.

[31] P. Strojan. Role of radiotherapy in melanoma management. *Radiol Oncol*, 44(1):1–12, 2010.

[32] E. Livingstone, L. Zimmer, J. Vaubel, and D. Schadendorf. BRAF, MEK and KIT inhibitors for melanoma: Adverse events and their management. *Chin Clin Oncol*, 3(3):29, 2014.

[33] A. D. Ballantyne and K. P. Garnock-Jones. Dabrafenib: First global approval. *Drugs*, 73(12):1367–76, 2013.

[34] D. Klinac, E. S. Gray, M. Millward, and M. Ziman. Advances in personalized targeted treatment of metastatic melanoma and non-invasive tumor monitoring. *Front Oncol*, 3:54, 2013.

[35] G. V. Long, U. Trefzer, M. A. Davies, R. F. Kefford, P. A. Ascierto, P. B. Chapman, I. Puzanov, A. Hauschild, C. Robert, A. Algazi, L. Mortier, H. Tawbi, T. Wilhelm, L. Zimmer, J. Switzky, S. Swann, A. M. Martin, M. Guckert, V. Goodman, M. Streit, J. M. Kirkwood, and D. Schadendorf. Dabrafenib in patients with Val600Glu or Val600Lys BRAF-mutant melanoma metastatic to the brain (BREAK-MB): A multicentre, open-label, phase 2 trial. *Lancet Oncol*, 13(11):1087–95, 2012.

[36] K. T. Flaherty, J. R. Infante, A. Daud, R. Gonzalez, R. F. Kefford, J. Sosman, O. Hamid, L. Schuchter, J. Cebon, N. Ibrahim, R. Kudchadkar, 3rd Burris, H. A., G. Falchook, A. Algazi, K. Lewis, G. V. Long, I. Puzanov, P. Lebowitz, A. Singh, S. Little, P. Sun, A. Allred, D. Ouellet, K. B. Kim, K. Patel, and J. Weber. Combined BRAF and MEK inhibition in melanoma with BRAF V600 mutations. *N Engl J Med*, 367(18):1694–703, 2012.

[37] B. S. Kalal, D. Upadhya, and V. R. Pai. Chemotherapy resistance mechanisms in advanced skin cancer. *Oncol Rev*, 11(1):326, 2017.

[38] M. Winder and A. Viros. Mechanisms of drug resistance in melanoma. *Handb Exp Pharmacol*, 249:91–108, 2018.

[39] S. Bhatia, S. S. Tykodi, and J. A. Thompson. Treatment of metastatic melanoma: An overview. *Oncology (Williston Park)*, 23(6):488–96, 2009.

[40] M. Sanlorenzo, I. Vujic, C. Posch, A. Dajee, A. Yen, S. Kim, M. Ashworth, M. D. Rosenblum, A. Algazi, S. Osella-Abate, P. Quaglino, A. Daud, and S. Ortiz-Urda. Melanoma immunotherapy. *Cancer Biol Ther*, 15(6):665–74, 2014.

[41] J. F. Brunet, F. Denizot, M. F. Luciani, M. Roux-Dosseto, M. Suzan, M. G. Mattei, and P. Golstein. A new member of the immunoglobulin superfamily–CTLA-4. *Nature*, 328(6127):267–70, 1987.

[42] P. Waterhouse, J. M. Penninger, E. Timms, A. Wakeham, A. Shahinian, K. P. Lee, C. B. Thompson, H. Griesser, and T. W. Mak. Lymphoproliferative disorders with early lethality in mice deficient in CTLA-4. *Science*, 270(5238):985–8, 1995.

[43] H. O. Alsaab, S. Sau, R. Alzhrani, K. Tatiparti, K. Bhise, S. K. Kashaw, and A. K. Iyer. PD-1 and PD-L1 checkpoint signaling inhibition for cancer immunotherapy: Mechanism, combinations, and clinical outcome. *Front Pharmacol*, 8:561, 2017.

[44] P. Specenier. Nivolumab in melanoma. *Expert Rev Anticancer Ther*, 16(12):1247–1261, 2016.

[45] C. Robert, J. Schachter, G. V. Long, A. Arance, J. J. Grob, L. Mortier, A. Daud, M. S. Carlino, C. McNeil, M. Lotem, J. Larkin, P. Lorigan, B. Neyns, C. U. Blank, O. Hamid, C. Mateus, R. Shapira-Frommer, M. Kosh, H. Zhou, N. Ibrahim, S. Ebbinghaus, A. Ribas, and Keynote investigators. Pembrolizumab versus Ipilimumab in advanced melanoma. *N Engl J Med*, 372(26):2521–32, 2015.

[46] S. L. Topalian, F. S. Hodi, J. R. Brahmer, S. N. Gettinger, D. C. Smith, D. F. McDermott, J. D. Powderly, R. D. Carvajal, J. A. Sosman, M. B. Atkins, P. D. Leming, D. R. Spigel, S. J. Antonia, L. Horn, C. G. Drake, D. M. Pardoll, L. Chen, W. H. Sharfman, R. A. Anders, J. M. Taube, T. L. McMiller, H. Xu, A. J. Korman, M. Jure-Kunkel, S. Agrawal, D. McDonald, G. D. Kollia, A. Gupta, J. M. Wigginton, and M. Sznol. Safety, activity, and immune correlates of anti-PD-1 antibody in cancer. *N Engl J Med*, 366(26):2443–54, 2012.

[47] J. Paik. Nivolumab Plus Relatlimab: First Approval. *Drugs*, 82(8):925–931, 2022.

[48] B. Huard, M. Tournier, T. Hercend, F. Triebel, and F. Faure. Lymphocyte-activation gene 3/major histocompatibility complex class ii interaction modulates the antigenic response of cd4+ t lymphocytes. *Eur J Immunol*, 24(12):3216–21, 1994.

[49] B. Huard, P. Prigent, F. Pages, D. Bruniquel, and F. Triebel. T cell major histocompatibility complex class ii molecules down-regulate cd4+ t cell clone responses following lag-3 binding. *Eur J Immunol*, 26(5):1180–6, 1996.

[50] Y. Wei and Z. Li. Lag3-pd-1 combo overcome the disadvantage of drug resistance. *Front Oncol*, 12:831407, 2022.

[51] H. A. Tawbi, D. Schadendorf, E. J. Lipson, P. A. Ascierto, L. Matamala, E. Castillo Gutierrez, P. Rutkowski, H. J. Gogas, C. D. Lao, J. J. De Menezes, S. Dalle, A. Arance, J. J. Grob, S. Srivastava, M. Abaskharoun, M. Hamilton,

S. Keidel, K. L. Simonsen, A. M. Sobiesk, B. Li, F. S. Hodi, G. V. Long, and Relativity Investigators. Relatlimab and Nivolumab versus Nivolumab in Untreated Advanced Melanoma. *N Engl J Med*, 386(1):24–34, 2022.

[52] J. Pol, G. Kroemer, and L. Galluzzi. First oncolytic virus approved for melanoma immunotherapy. *Oncoimmunology*, 5(1):e1115641, 2016.

[53] J. Yuan, G. Y. Ku, H. F. Gallardo, F. Orlandi, G. Manukian, T. S. Rasalan, Y. Xu, H. Li, S. Vyas, Z. Mu, P. B. Chapman, S. E. Krown, K. Panageas, S. L. Terzulli, L. J. Old, A. N. Houghton, and J. D. Wolchok. Safety and immunogenicity of a human and mouse gp100 DNA vaccine in a phase I trial of patients with melanoma. *Cancer Immun*, 9:5, 2009.

[54] H. Kanzler, F. J. Barrat, E. M. Hessel, and R. L. Coffman. Therapeutic targeting of innate immunity with Toll-like receptor agonists and antagonists. *Nat Med*, 13(5):552–9, 2007.

[55] M. E. Dudley, J. C. Yang, R. Sherry, M. S. Hughes, R. Royal, U. Kammula, P. F. Robbins, J. Huang, D. E. Citrin, S. F. Leitman, J. Wunderlich, N. P. Restifo, A. Thomasian, S. G. Downey, F. O. Smith, J. Klapper, K. Morton, C. Laurencot, D. E. White, and S. A. Rosenberg. Adoptive cell therapy for patients with metastatic melanoma: evaluation of intensive myeloablative chemoradiation preparative regimens. *J Clin Oncol*, 26(32):5233–9, 2008.

[56] D. Hanahan and R. A. Weinberg. Hallmarks of cancer: The next generation. *Cell*, 144(5):646–74, 2011.

[57] D. A. Vignali, L. W. Collison, and C. J. Workman. How regulatory T cells work. *Nat Rev Immunol*, 8(7):523–32, 2008.

[58] E. M. Shevach. Foxp3(+) T regulatory cells: Still many unanswered questions - A perspective after 20 years of study. *Front Immunol*, 9:1048, 2018.

[59] H. Kawamoto and N. Minato. Myeloid cells. *Int J Biochem Cell Biol*, 36(8):1374–9, 2004.

[60] V. Umansky, A. Sevko, C. Gebhardt, and J. Utikal. Myeloid-derived suppressor cells in malignant melanoma. *J Dtsch Dermatol Ges*, 12(11):1021–7, 2014.

[61] D. G. Mairhofer, D. Ortner, C. H. Tripp, S. Schaffenrath, V. Fleming, L. Heger, K. Komenda, D. Reider, D. Dudziak, S. Chen, J. C. Becker, V. Flacher, and P. Stoitzner. Impaired gp100-Specific CD8(+) T-cell responses in the presence of myeloid-derived suppressor cells in a spontaneous mouse melanoma model. *J Invest Dermatol*, 135(11):2785–2793, 2015.

[62] K. R. Jordan, R. N. Amaria, O. Ramirez, E. B. Callihan, D. Gao, M. Borakove, E. Manthey, V. F. Borges, and M. D. McCarter. Myeloid-derived suppressor cells are associated with disease progression and decreased overall survival in advanced-stage melanoma patients. *Cancer Immunol Immunother*, 62(11):1711–22, 2013.

[63] T. Fujimura, Y. Kambayashi, Y. Fujisawa, T. Hidaka, and S. Aiba. Tumor-associated macrophages: Therapeutic targets for skin cancer. *Front Oncol*, 8:3, 2018.

[64] R. Noy and J. W. Pollard. Tumor-associated macrophages: From mechanisms to therapy. *Immunity*, 41(1):49–61, 2014.

[65] T. Fujimura, S. Ring, V. Umansky, K. Mahnke, and A. H. Enk. Regulatory T cells stimulate B7-H1 expression in myeloid-derived suppressor cells in ret melanomas. *J Invest Dermatol*, 132(4):1239–46, 2012.

[66] M. Baay, A. Brouwer, P. Pauwels, M. Peeters, and F. Lardon. Tumor cells and tumor-associated macrophages: secreted proteins as potential targets for therapy. *Clin Dev Immunol*, 2011:565187, 2011.

[67] M. Wieczorek, E. T. Abualrous, J. Sticht, M. Alvaro-Benito, S. Stolzenberg, F. Noe, and C. Freund. Major Histocompatibility Complex (MHC) Class I and MHC Class II proteins: Conformational plasticity in antigen presentation. *Front Immunol*, 8:292, 2017.

[68] J. Neefjes, M. L. Jongsma, P. Paul, and O. Bakke. Towards a systems understanding of MHC class I and MHC class II antigen presentation. *Nat Rev Immunol*, 11(12):823–36, 2011.

[69] J. M. Vyas, A. G. Van der Veen, and H. L. Ploegh. The known unknowns of antigen processing and presentation. *Nat Rev Immunol*, 8(8):607–18, 2008.

[70] E. W. Hewitt. The MHC class I antigen presentation pathway: Strategies for viral immune evasion. *Immunology*, 110(2):163–9, 2003.

[71] F. R. Schumacher, L. Delamarre, S. Jhunjhunwala, Z. Modrusan, Q. T. Phung, J. E. Elias, and J. R. Lill. Building proteomic tool boxes to monitor MHC class I and class II peptides. *Proteomics*, 17(1-2), 2017.

[72] P. Leone, E. C. Shin, F. Perosa, A. Vacca, F. Dammacco, and V. Racanelli. MHC class I antigen processing and presenting machinery: Organization, function, and defects in tumor cells. *J Natl Cancer Inst*, 105(16):1172–87, 2013.

[73] A. Ciechanover. Intracellular protein degradation: From a vague idea thru the lysosome and the ubiquitin-proteasome system and onto human diseases and drug targeting. *Biochim Biophys Acta*, 1824(1):3–13, 2012.

[74] J. W. Yewdell. Not such a dismal science: The economics of protein synthesis, folding, degradation and antigen processing. *Trends Cell Biol*, 11(7):294–7, 2001.

[75] U. Schubert, L. C. Anton, J. Gibbs, C. C. Norbury, J. W. Yewdell, and J. R. Bennink. Rapid degradation of a large fraction of newly synthesized proteins by proteasomes. *Nature*, 404(6779):770–4, 2000.

[76] A. L. Goldberg and J. F. Dice. Intracellular protein degradation in mammalian and bacterial cells. *Annu Rev Biochem*, 43(0):835–69, 1974.

[77] A. L. Goldberg. Protein degradation and protection against misfolded or damaged proteins. *Nature*, 426(6968):895–9, 2003.

[78] A. Craiu, T. Akopian, A. Goldberg, and K. L. Rock. Two distinct proteolytic processes in the generation of a major histocompatibility complex class I-presented peptide. *Proc Natl Acad Sci U S A*, 94(20):10850–5, 1997.

[79] N. Brouwenstijn, T. Serwold, and N. Shastri. MHC class I molecules can direct proteolytic cleavage of antigenic precursors in the endoplasmic reticulum. *Immunity*, 15(1):95–104, 2001.

[80] D. Fruci, G. Niedermann, R. H. Butler, and P. M. van Endert. Efficient MHC class I-independent amino-terminal trimming of epitope precursor peptides in the endoplasmic reticulum. *Immunity*, 15(3):467–76, 2001.

[81] S. C. Chang, F. Momburg, N. Bhutani, and A. L. Goldberg. The ER aminopeptidase, ERAP1, trims precursors to lengths of MHC class I peptides by a "molecular ruler" mechanism. *Proc Natl Acad Sci U S A*, 102(47):17107–12, 2005.

[82] T. Saric, S. C. Chang, A. Hattori, I. A. York, S. Markant, K. L. Rock, M. Tsujimoto, and A. L. Goldberg. An IFN-gamma-induced aminopeptidase in the ER, ERAP1, trims precursors to MHC class I-presented peptides. *Nat Immunol*, 3(12):1169–76, 2002.

[83] M. J. Androlewicz, K. S. Anderson, and P. Cresswell. Evidence that transporters associated with antigen processing translocate a major histocompatibility complex class I-binding peptide into the endoplasmic reticulum in an ATP-dependent manner. *Proc Natl Acad Sci U S A*, 90(19):9130–4, 1993.

[84] J. J. Neefjes, F. Momburg, and G. J. Hammerling. Selective and ATP-dependent translocation of peptides by the MHC-encoded transporter. *Science*, 261(5122):769–71, 1993.

[85] M. Gromme and J. Neefjes. Antigen degradation or presentation by MHC class I molecules via classical and non-classical pathways. *Mol Immunol*, 39(3-4):181–202, 2002.

[86] L. Schmitt and R. Tampe. Structure and mechanism of ABC transporters. *Curr Opin Struct Biol*, 12(6):754–60, 2002.

[87] S. Arora, P. E. Lapinski, and M. Raghavan. Use of chimeric proteins to investigate the role of transporter associated with antigen processing (TAP) structural domains in peptide binding and translocation. *Proc Natl Acad Sci U S A*, 98(13):7241–6, 2001.

[88] P. M. van Endert, R. Tampe, T. H. Meyer, R. Tisch, J. F. Bach, and H. O. McDevitt. A sequential model for peptide binding and transport by the transporters associated with antigen processing. *Immunity*, 1(6):491–500, 1994.

[89] J. Roelse, M. Gromme, F. Momburg, G. Hammerling, and J. Neefjes. Trimming of TAP-translocated peptides in the endoplasmic reticulum and in the cytosol during recycling. *J Exp Med*, 180(5):1591–7, 1994.

[90] P. A. Wearsch and P. Cresswell. The quality control of MHC class I peptide loading. *Curr Opin Cell Biol*, 20(6):624–31, 2008.

[91] C. Hammond, I. Braakman, and A. Helenius. Role of N-linked oligosaccharide recognition, glucose trimming, and calnexin in glycoprotein folding and quality control. *Proc Natl Acad Sci U S A*, 91(3):913–7, 1994.

[92] I. Wada, S. Imai, M. Kai, F. Sakane, and H. Kanoh. Chaperone function of calreticulin when expressed in the endoplasmic reticulum as the membrane-anchored and soluble forms. *J Biol Chem*, 270(35):20298–304, 1995.

[93] J. D. Oliver, H. L. Roderick, D. H. Llewellyn, and S. High. ERp57 functions as a subunit of specific complexes formed with the ER lectins calreticulin and calnexin. *Mol Biol Cell*, 10(8):2573–82, 1999.

[94] L. Ellgaard and A. Helenius. ER quality control: Towards an understanding at the molecular level. *Curr Opin Cell Biol*, 13(4):431–7, 2001.

[95] E. Degen, M. F. Cohen-Doyle, and D. B. Williams. Efficient dissociation of the p88 chaperone from major histocompatibility complex class I molecules requires both beta 2-microglobulin and peptide. *J Exp Med*, 175(6):1653–61, 1992.

[96] B. Sadasivan, P. J. Lehner, B. Ortmann, T. Spies, and P. Cresswell. Roles for calreticulin and a novel glycoprotein, tapasin, in the interaction of MHC class I molecules with TAP. *Immunity*, 5(2):103–14, 1996.

[97] P. J. Lehner, M. J. Surman, and P. Cresswell. Soluble tapasin restores MHC class I expression and function in the tapasin-negative cell line .220. *Immunity*, 8(2):221–31, 1998.

[98] B. Ortmann, J. Copeman, P. J. Lehner, B. Sadasivan, J. A. Herberg, A. G. Grandea, S. R. Riddell, R. Tampe, T. Spies, J. Trowsdale, and P. Cresswell. A critical role for tapasin in the assembly and function of multimeric MHC class I-TAP complexes. *Science*, 277(5330):1306–9, 1997.

[99] 3rd Grandea, A. G., P. J. Lehner, P. Cresswell, and T. Spies. Regulation of MHC class I heterodimer stability and interaction with TAP by tapasin. *Immunogenetics*, 46(6):477–83, 1997.

[100] A. P. Williams, C. A. Peh, A. W. Purcell, J. McCluskey, and T. Elliott. Optimization of the MHC class I peptide cargo is dependent on tapasin. *Immunity*, 16(4):509–20, 2002.

[101] K. Dhatchinamoorthy, J. D. Colbert, and K. L. Rock. Cancer immune evasion through loss of MHC Class I antigen presentation. *Front Immunol*, 12:636568, 2021.

[102] A. M. Cornel, I. L. Mimpen, and S. Nierkens. MHC Class I downregulation in cancer: Underlying mechanisms and potential targets for cancer immunotherapy. *Cancers (Basel)*, 12(7), 2020.

[103] T. Kageshita, S. Hirai, T. Ono, D. J. Hicklin, and S. Ferrone. Down-regulation of HLA class I antigen-processing molecules in malignant melanoma: Association with disease progression. *Am J Pathol*, 154(3):745–54, 1999.

[104] J. Kamarashev, S. Ferrone, B. Seifert, R. Boni, F. O. Nestle, G. Burg, and R. Dummer. TAP1 down-regulation in primary melanoma lesions: An independent marker of poor prognosis. *Int J Cancer*, 95(1):23–8, 2001.

[105] J. Dissemond, P. Gotte, J. Mors, A. Lindeke, M. Goos, S. Ferrone, and S. N. Wagner. Association of TAP1 downregulation in human primary melanoma lesions with lack of spontaneous regression. *Melanoma Res*, 13(3):253–8, 2003.

[106] B. Seliger, U. Ritz, R. Abele, M. Bock, R. Tampe, G. Sutter, I. Drexler, C. Huber, and S. Ferrone. Immune escape of melanoma: first evidence of structural alterations in two distinct components of the MHC class I antigen processing pathway. *Cancer Res*, 61(24):8647–50, 2001.

[107] T. Yang, B. A. McNally, S. Ferrone, Y. Liu, and P. Zheng. A single-nucleotide deletion leads to rapid degradation of TAP-1 mRNA in a melanoma cell line. *J Biol Chem*, 278(17):15291–6, 2003.

[108] A. Respa, J. Bukur, S. Ferrone, G. Pawelec, Y. Zhao, E. Wang, F. M. Marincola, and B. Seliger. Association of IFN-gamma signal transduction defects with impaired HLA class I antigen processing in melanoma cell lines. *Clin Cancer Res*, 17(9):2668–78, 2011.

[109] E. Kamphausen, C. Kellert, T. Abbas, N. Akkad, S. Tenzer, G. Pawelec, H. Schild, P. van Endert, and B. Seliger. Distinct molecular mechanisms leading to deficient expression of ER-resident aminopeptidases in melanoma. *Cancer Immunol Immunother*, 59(8):1273–84, 2010.

[110] T. Cabrera, I. Maleno, A. Collado, M. A. Lopez Nevot, B. D. Tait, and F. Garrido. Analysis of HLA class I alterations in tumors: Choosing a strategy based on known patterns of underlying molecular mechanisms. *Tissue Antigens*, 69 Suppl 1:264–8, 2007.

[111] R. Benitez, D. Godelaine, M. A. Lopez-Nevot, F. Brasseur, P. Jimenez, M. Marchand, M. R. Oliva, N. van Baren, T. Cabrera, G. Andry, C. Landry, F. Ruiz-Cabello, T. Boon, and F. Garrido. Mutations of the beta2-microglobulin gene result in a lack of HLA class I molecules on melanoma cells of two patients immunized with MAGE peptides. *Tissue Antigens*, 52(6):520–9, 1998.

[112] D. J. Hicklin, Z. Wang, F. Arienti, L. Rivoltini, G. Parmiani, and S. Ferrone. Beta2-Microglobulin mutations, HLA class I antigen loss, and tumor progression in melanoma. *J Clin Invest*, 101(12):2720–9, 1998.

[113] A. Serrano, S. Tanzarella, I. Lionello, R. Mendez, C. Traversari, F. Ruiz-Cabello, and F. Garrido. Rexpression of HLA class I antigens and restoration of antigen-specific CTL response in melanoma cells following 5-aza-2'-deoxycytidine treatment. *Int J Cancer*, 94(2):243–51, 2001.

[114] C. A. White, S. A. Thomson, L. Cooper, P. M. van Endert, R. Tampe, B. Coupar, L. Qiu, P. G. Parsons, D. J. Moss, and R. Khanna. Constitutive transduction of peptide transporter and HLA genes restores antigen processing function and cytotoxic T cell-mediated immune recognition of human melanoma cells. *Int J Cancer*, 75(4):590–5, 1998.

[115] C. S. Grasso, J. Tsoi, M. Onyshchenko, G. Abril-Rodriguez, P. Ross-Macdonald, M. Wind-Rotolo, A. Champhekar, E. Medina, D. Y. Torrejon, D. S. Shin, P. Tran, Y. J. Kim, C. Puig-Saus, K. Campbell, A. Vega-Crespo, M. Quist, C. Martignier, J. J. Luke, J. D. Wolchok, D. B. Johnson, B. Chmielowski, F. S. Hodi, S. Bhatia, W. Sharfman, W. J. Urba, Jr. Slingluff, C. L., A. Diab, Jbag Haanen, S. M. Algarra, D. M. Pardoll, V. Anagnostou, S. L. Topalian, V. E. Velculescu, D. E. Speiser, A. Kalbasi, and A. Ribas. Conserved interferon-gamma signaling drives clinical response to immune checkpoint blockade therapy in melanoma. *Cancer Cell*, 38(4):500–515 e3, 2020.

[116] F. Zhou. Molecular mechanisms of IFN-gamma to up-regulate MHC class I antigen processing and presentation. *Int Rev Immunol*, 28(3-4):239–60, 2009.

[117] T. E. Angell, M. G. Lechner, J. K. Jang, J. S. LoPresti, and A. L. Epstein. MHC class I loss is a frequent mechanism of immune escape in papillary thyroid cancer that is reversed by interferon and selumetinib treatment in vitro. *Clin Cancer Res*, 20(23):6034–44, 2014.

[118] L. Mora-Garcia Mde, A. Duenas-Gonzalez, J. Hernandez-Montes, E. De la Cruz-Hernandez, E. Perez-Cardenas, B. Weiss-Steider, E. Santiago-Osorio, V. F. Ortiz-Navarrete, V. H. Rosales, D. Cantu, M. Lizano-Soberon, M. P. Rojo-Aguilar, and A. Monroy-Garcia. Up-regulation of HLA class-I antigen expression and antigen-specific CTL response in cervical cancer cells by the demethylating agent hydralazine and the histone deacetylase inhibitor valproic acid. *J Transl Med*, 4:55, 2006.

[119] P. J. van den Elsen, T. M. Holling, N. van der Stoep, and J. M. Boss. DNA methylation and expression of major histocompatibility complex class I and class II transactivator genes in human developmental tumor cells and in T cell malignancies. *Clin Immunol*, 109(1):46–52, 2003.

[120] H. Li, K. B. Chiappinelli, A. A. Guzzetta, H. Easwaran, R. W. Yen, R. Vatapalli, M. J. Topper, J. Luo, R. M. Connolly, N. S. Azad, V. Stearns, D. M. Pardoll, N. Davidson, P. A. Jones, D. J. Slamon, S. B. Baylin, C. A. Zahnow, and N. Ahuja. Immune regulation by low doses of the DNA methyltransferase inhibitor 5-azacitidine in common human epithelial cancers. *Oncotarget*, 5(3):587–98, 2014.

[121] S. Oshima, T. Nakamura, S. Namiki, E. Okada, K. Tsuchiya, R. Okamoto, M. Yamazaki, T. Yokota, M. Aida, Y. Yamaguchi, T. Kanai, H. Handa, and M. Watanabe. Interferon regulatory factor 1 (IRF-1) and IRF-2 distinctively up-regulate gene expression and production of interleukin-7 in human intestinal epithelial cells. *Mol Cell Biol*, 24(14):6298–310, 2004.

[122] D. J. Propper, D. Chao, J. P. Braybrooke, P. Bahl, P. Thavasu, F. Balkwill, H. Turley, N. Dobbs, K. Gatter, D. C. Talbot, A. L. Harris, and T. S. Ganesan. Low-dose IFN-gamma induces tumor MHC expression in metastatic malignant melanoma. *Clin Cancer Res*, 9(1):84–92, 2003.

[123] V. Vlkova, I. Stepanek, V. Hruskova, F. Senigl, V. Mayerova, M. Sramek, J. Simova, J. Bieblova, M. Indrova, T. Hejhal, N. Derian, D. Klatzmann, A. Six, and M. Reinis. Epigenetic regulations in the IFNgamma signalling pathway: IFNgamma-mediated MHC class I upregulation on tumour cells is associated with DNA demethylation of antigen-presenting machinery genes. *Oncotarget*, 5(16):6923–35, 2014.

[124] N. Luo, M. J. Nixon, P. I. Gonzalez-Ericsson, V. Sanchez, S. R. Opalenik, H. Li, C. A. Zahnow, M. L. Nickels, F. Liu, M. N. Tantawy, M. E. Sanders, H. C. Manning,

and J. M. Balko. DNA methyltransferase inhibition upregulates MHC-I to potentiate cytotoxic T lymphocyte responses in breast cancer. *Nat Commun*, 9(1):248, 2018.

[125] E. Fonsatti, H. J. Nicolay, L. Sigalotti, L. Calabro, L. Pezzani, F. Colizzi, M. Altomonte, M. Guidoboni, F. M. Marincola, and M. Maio. Functional up-regulation of human leukocyte antigen class I antigens expression by 5-aza-2'-deoxycytidine in cutaneous melanoma: Immunotherapeutic implications. *Clin Cancer Res*, 13(11):3333–8, 2007.

[126] F. J. Slack and A. M. Chinnaiyan. The role of non-coding RNAs in oncology. *Cell*, 179(5):1033–1055, 2019.

[127] K. A. Marijt, S. H. Van Der Burg, and T. van Hall. TEIPP peptides: exploration of unTAPped cancer antigens. *Oncoimmunology*, 8(8):1599639, 2019.

[128] K. Mimura, K. Shiraishi, A. Mueller, S. Izawa, L. F. Kua, J. So, W. P. Yong, H. Fujii, B. Seliger, R. Kiessling, and K. Kono. The MAPK pathway is a predominant regulator of HLA-A expression in esophageal and gastric cancer. *J Immunol*, 191(12):6261–72, 2013.

[129] E. J. Brea, C. Y. Oh, E. Manchado, S. Budhu, R. S. Gejman, G. Mo, P. Mondello, J. E. Han, C. A. Jarvis, D. Ulmert, Q. Xiang, A. Y. Chang, R. J. Garippa, T. Merghoub, J. D. Wolchok, N. Rosen, S. W. Lowe, and D. A. Scheinberg. Kinase regulation of human MHC Class I molecule expression on cancer cells. *Cancer Immunol Res*, 4(11):936–947, 2016.

[130] C. Y. Oh, M. G. Klatt, C. Bourne, T. Dao, M. M. Dacek, E. J. Brea, S. S. Mun, A. Y. Chang, T. Korontsvit, and D. A. Scheinberg. ALK and RET inhibitors promote HLA Class I antigen presentation and unmask new antigens within the tumor immunopeptidome. *Cancer Immunol Res*, 7(12):1984–1997, 2019.

[131] A. Bartolomucci, R. Possenti, S. K. Mahata, R. Fischer-Colbrie, Y. P. Loh, and S. R. Salton. The extended granin family: structure, function, and biomedical implications. *Endocr Rev*, 32(6):755–97, 2011.

[132] S. K. Mahata, C. A. Kozak, J. Szpirer, C. Szpirer, W. S. Modi, H. H. Gerdes, W. B. Huttner, and D. T. O'Connor. Dispersion of chromogranin/secretogranin secretory protein family loci in mammalian genomes. *Genomics*, 33(1):135–9, 1996.

[133] R. Kirchmair, R. Hogue-Angeletti, J. Gutierrez, R. Fischer-Colbrie, and H. Winkler. Secretoneurin–a neuropeptide generated in brain, adrenal medulla and other endocrine tissues by proteolytic processing of secretogranin II (chromogranin C). *Neuroscience*, 53(2):359–65, 1993.

[134] M. Montero-Hadjadje, G. Pelletier, L. Yon, S. Li, J. Guillemot, R. Magoul, Y. Tillet, H. Vaudry, and Y. Anouar. Biochemical characterization and immunocytochemical localization of EM66, a novel peptide derived from secretogranin II, in the rat pituitary and adrenal glands. *J Histochem Cytochem*, 51(8):1083–95, 2003.

[135] A. Yajima, M. Ikeda, K. Miyazaki, T. Maeshima, N. Narita, and M. Narita. Manserin, a novel peptide from secretogranin II in the neuroendocrine system. *Neuroreport*, 15(11):1755–9, 2004.

[136] M. Courel, F. Z. El Yamani, D. Alexandre, H. El Fatemi, C. Delestre, M. Montero-Hadjadje, F. Tazi, A. Amarti, R. Magoul, N. Chartrel, and Y. Anouar. Secretogranin II is overexpressed in advanced prostate cancer and promotes the neuroendocrine differentiation of prostate cancer cells. *Eur J Cancer*, 50(17):3039–49, 2014.

[137] M. Montero-Hadjadje, S. Vaingankar, S. Elias, H. Tostivint, S. K. Mahata, and Y. Anouar. Chromogranins A and B and secretogranin II: Evolutionary and functional aspects. *Acta Physiol (Oxf)*, 192(2):309–24, 2008.

[138] M. Courel, A. Soler-Jover, J. L. Rodriguez-Flores, S. K. Mahata, S. Elias, M. Montero-Hadjadje, Y. Anouar, R. J. Giuly, D. T. O'Connor, and L. Taupenot. Pro-hormone secretogranin II regulates dense core secretory granule biogenesis in catecholaminergic cells. *J Biol Chem*, 285(13):10030–10043, 2010.

[139] M. J. Kuehn, J. M. Herrmann, and R. Schekman. COPII-cargo interactions direct protein sorting into ER-derived transport vesicles. *Nature*, 391(6663):187–90, 1998.

[140] T. Kim, M. C. Gondre-Lewis, I. Arnaoutova, and Y. P. Loh. Dense-core secretory granule biogenesis. *Physiology (Bethesda)*, 21:124–33, 2006.

[141] H. H. Gerdes and M. M. Glombik. Signal-mediated sorting of chromogranins to secretory granules. *Adv Exp Med Biol*, 482:41–54, 2000.

[142] A. Rustom, M. Bajohrs, C. Kaether, P. Keller, D. Toomre, D. Corbeil, and H. H. Gerdes. Selective delivery of secretory cargo in Golgi-derived carriers of nonepithelial cells. *Traffic*, 3(4):279–88, 2002.

[143] M. Courel, M. S. Vasquez, V. Y. Hook, S. K. Mahata, and L. Taupenot. Sorting of the neuroendocrine secretory protein Secretogranin II into the regulated secretory pathway: Role of N- and C-terminal alpha-helical domains. *J Biol Chem*, 283(17):11807–22, 2008.

[144] K. Hotta, M. Hosaka, A. Tanabe, and T. Takeuchi. Secretogranin II binds to secretogranin III and forms secretory granules with orexin, neuropeptide Y, and POMC. *J Endocrinol*, 202(1):111–21, 2009.

[145] J. Guillemot, E. Thouennon, M. Guerin, V. Vallet-Erdtmann, A. Ravni, M. Montero-Hadjadje, H. Lefebvre, M. Klein, M. Muresan, N. G. Seidah, Y. Anouar, and L. Yon. Differential expression and processing of secretogranin II in relation to the status of pheochromocytoma: Implications for the production of the tumoral marker EM66. *J Mol Endocrinol*, 48(2):115–27, 2012.

[146] L. Yon, J. Guillemot, M. Montero-Hadjadje, L. Grumolato, J. Leprince, H. Lefebvre, V. Contesse, P. F. Plouin, H. Vaudry, and Y. Anouar. Identification of the secretogranin II-derived peptide EM66 in pheochromocytomas as a potential marker for discriminating benign versus malignant tumors. *J Clin Endocrinol Metab*, 88(6):2579–85, 2003.

[147] J. Guillemot, Y. Anouar, M. Montero-Hadjadje, E. Grouzmann, L. Grumolato, J. Roshmaninho-Salgado, V. Turquier, C. Duparc, H. Lefebvre, P. F. Plouin, M. Klein, M. Muresan, B. K. Chow, H. Vaudry, and L. Yon. Circulating EM66 is a highly sensitive marker for the diagnosis and follow-up of pheochromocytoma. *Int J Cancer*, 118(8):2003–12, 2006.

[148] M. Stridsberg, B. Eriksson, and E. T. Janson. Measurements of secretogranins II, III, V and proconvertases 1/3 and 2 in plasma from patients with neuroendocrine tumours. *Regul Pept*, 148(1-3):95–8, 2008.

[149] L. Li, A. C. Hung, and A. G. Porter. Secretogranin II: A key AP-1-regulated protein that mediates neuronal differentiation and protection from nitric oxide-induced apoptosis of neuroblastoma cells. *Cell Death Differ*, 15(5):879–88, 2008.

[150] J. W. Liu, F. Yu, Y. F. Tan, J. P. Huo, Z. Liu, X. J. Wang, and J. M. Li. Profiling of tumor microenvironment components identifies five stroma-related genes with prognostic implications in colorectal cancer. *Cancer Biother Radiopharm*, 2020.

[151] G. Sun, Y. Li, Y. Peng, D. Lu, F. Zhang, X. Cui, Q. Zhang, and Z. Li. Identification of a five-gene signature with prognostic value in colorectal cancer. *J Cell Physiol*, 234(4):3829–3836, 2019.

[152] C. Fang, L. Dai, C. Wang, C. Fan, Y. Yu, L. Yang, H. Deng, and Z. Zhou. Secretogranin II impairs tumor growth and angiogenesis by promoting degradation of hypoxia-inducible factor-1alpha in colorectal cancer. *Mol Oncol*, 2021.

[153] P. R. Hannon, D. M. Duffy, K. L. Rosewell, M. Brannstrom, J. W. Akin, and Jr. Curry, T. E. Ovulatory induction of SCG2 in human, nonhuman primate, and rodent granulosa cells stimulates ovarian angiogenesis. *Endocrinology*, 159(6):2447–2458, 2018.

[154] M. J. Luo, S. S. Rao, Y. J. Tan, H. Yin, X. K. Hu, Y. Zhang, Y. W. Liu, T. Yue, L. J. Chen, L. Li, Y. R. Huang, Y. X. Qian, Z. Z. Liu, J. Cao, Z. X. Wang, Z. W. Luo, Y. Y. Wang, K. Xia, S. Y. Tang, C. Y. Chen, and H. Xie. Fasting before or after wound injury accelerates wound healing through the activation of pro-angiogenic SMOC1 and SCG2. *Theranostics*, 10(8):3779–3792, 2020.

[155] W. K. Peitsch, Y. Doerflinger, R. Fischer-Colbrie, V. Huck, A. T. Bauer, J. Utikal, S. Goerdt, and S. W. Schneider. Desmoglein 2 depletion leads to increased migration and upregulation of the chemoattractant secretoneurin in melanoma cells. *PLoS One*, 9(2):e89491, 2014.

[156] A. Federico, T. Steinfass, L. Larribere, D. Novak, F. Moris, L. E. Nunez, V. Umansky, and J. Utikal. Mithramycin A and Mithralog EC-8042 inhibit SETDB1 expression and its oncogenic activity in malignant melanoma. *Mol Ther Oncolytics*, 18:83–99, 2020.

[157] L. A. Johnson, B. Heemskerk, Jr. Powell, D. J., C. J. Cohen, R. A. Morgan, M. E. Dudley, P. F. Robbins, and S. A. Rosenberg. Gene transfer of tumor-reactive TCR confers both high avidity and tumor reactivity to nonreactive peripheral blood mononuclear cells and tumor-infiltrating lymphocytes. *J Immunol*, 177(9):6548–59, 2006.

[158] N. B. Wagner, B. Weide, M. Reith, K. Tarnanidis, C. Kehrel, R. Lichtenberger, A. Pflugfelder, E. Herpel, J. Eubel, K. Ikenberg, C. Busch, T. Holland-Letz, H. Naeher, C. Garbe, V. Umansky, A. Enk, J. Utikal, and C. Gebhardt. Diminished levels

of the soluble form of RAGE are related to poor survival in malignant melanoma. *Int J Cancer*, 137(11):2607–17, 2015.

[159] R Core Team. R: A language and environment for statistical computing. *R Foundation for Statistical Computing*, 2020. `https://www.r-project.org/`.

[160] G. K. Smyth. Linear models and empirical bayes methods for assessing differential expression in microarray experiments. *Stat Appl Genet Mol Biol*, 3:Article3, 2004.

[161] G. K. Smyth. limma: Linear models for microarray data. *Bioinformatics and Computational Biology Solutions Using R and Bioconductor*, pages 397–420, 2005.

[162] D. Wu and G. K. Smyth. Camera: A competitive gene set test accounting for inter-gene correlation. *Nucleic Acids Res*, 40(17):e133, 2012.

[163] M. Kanehisa and S. Goto. KEGG: Kyoto encyclopedia of genes and genomes. *Nucleic Acids Res*, 28(1):27–30, 2000.

[164] A. Fabregat, S. Jupe, L. Matthews, K. Sidiropoulos, M. Gillespie, P. Garapati, R. Haw, B. Jassal, F. Korninger, B. May, M. Milacic, C. D. Roca, K. Rothfels, C. Sevilla, V. Shamovsky, S. Shorser, T. Varusai, G. Viteri, J. Weiser, G. Wu, L. Stein, H. Hermjakob, and P. D'Eustachio. The Reactome pathway knowledgebase. *Nucleic Acids Res*, 46(D1):D649–D655, 2018.

[165] The Gene Ontology Consortium. Expansion of the gene ontology knowledgebase and resources. *Nucleic Acids Res*, 45(D1):D331–D338, 2017.

[166] A. I. Riker, S. A. Enkemann, O. Fodstad, S. Liu, S. Ren, C. Morris, Y. Xi, P. Howell, B. Metge, R. S. Samant, L. A. Shevde, W. Li, S. Eschrich, A. Daud, J. Ju, and J. Matta. The gene expression profiles of primary and metastatic melanoma yields a transition point of tumor progression and metastasis. *BMC Med Genomics*, 1:13, 2008.

[167] D. Liu, B. Schilling, D. Liu, A. Sucker, E. Livingstone, L. Jerby-Arnon, L. Zimmer, R. Gutzmer, I. Satzger, C. Loquai, S. Grabbe, N. Vokes, C. A. Margolis, J. Conway, M. X. He, H. Elmarakeby, F. Dietlein, D. Miao, A. Tracy, H. Gogas, S. M. Goldinger, J. Utikal, C. U. Blank, R. Rauschenberg, D. von Bubnoff, A. Krackhardt, B. Weide, S. Haferkamp, F. Kiecker, B. Izar, L. Garraway, A. Regev, K. Flaherty, A. Paschen, E. M. Van Allen, and D. Schadendorf. Integrative molecular and clinical modeling

of clinical outcomes to PD1 blockade in patients with metastatic melanoma. *Nat Med*, 25(12):1916–1927, 2019.

[168] E. Orouji, A. Federico, L. Larribere, D. Novak, D. B. Lipka, Y. Assenov, S. Sachindra, L. Huser, K. Granados, C. Gebhardt, C. Plass, V. Umansky, and J. Utikal. Histone methyltransferase SETDB1 contributes to melanoma tumorigenesis and serves as a new potential therapeutic target. *Int J Cancer*, 145(12):3462–3477, 2019.

[169] H. Wang, J. Yin, Y. Hong, A. Ren, H. Wang, M. Li, Q. Zhao, C. Jiang, and L. Liu. SCG2 is a prognostic biomarker associated with immune infiltration and macrophage polarization in colorectal cancer. *Front Cell Dev Biol*, 9:795133, 2021.

[170] E. Shklovskaya, J. H. Lee, S. Y. Lim, A. Stewart, B. Pedersen, P. Ferguson, R. P. Saw, J. F. Thompson, B. Shivalingam, M. S. Carlino, R. A. Scolyer, A. M. Menzies, G. V. Long, R. F. Kefford, and H. Rizos. Tumor MHC expression guides first-line immunotherapy selection in melanoma. *Cancers (Basel)*, 12(11), 2020.

[171] E. Shklovskaya and H. Rizos. MHC Class I deficiency in solid tumors and therapeutic strategies to overcome it. *Int J Mol Sci*, 22(13), 2021.

[172] S. Ito, S. Okano, M. Morita, H. Saeki, S. Tsutsumi, H. Tsukihara, Y. Nakashima, K. Ando, Y. Imamura, K. Ohgaki, E. Oki, H. Kitao, K. Mimori, and Y. Maehara. Expression of PD-L1 and HLA Class I in esophageal squamous cell carcinoma: prognostic factors for patient outcome. *Ann Surg Oncol*, 23(Suppl 4):508–515, 2016.

[173] S. Gettinger, J. Choi, K. Hastings, A. Truini, I. Datar, R. Sowell, A. Wurtz, W. Dong, G. Cai, M. A. Melnick, V. Y. Du, J. Schlessinger, S. B. Goldberg, A. Chiang, M. F. Sanmamed, I. Melero, J. Agorreta, L. M. Montuenga, R. Lifton, S. Ferrone, P. Kavathas, D. L. Rimm, S. M. Kaech, K. Schalper, R. S. Herbst, and K. Politi. Impaired HLA Class I antigen processing and presentation as a mechanism of acquired resistance to immune checkpoint inhibitors in lung cancer. *Cancer Discov*, 7(12):1420–1435, 2017.

[174] J. H. Lee, E. Shklovskaya, S. Y. Lim, M. S. Carlino, A. M. Menzies, A. Stewart, B. Pedersen, M. Irvine, S. Alavi, J. Y. H. Yang, D. Strbenac, R. P. M. Saw, J. F. Thompson, J. S. Wilmott, R. A. Scolyer, G. V. Long, R. F. Kefford, and H. Rizos. Transcriptional downregulation of MHC class I and melanoma de-differentiation in resistance to PD-1 inhibition. *Nat Commun*, 11(1):1897, 2020.

[175] M. Sade-Feldman, Y. J. Jiao, J. H. Chen, M. S. Rooney, M. Barzily-Rokni, J. P. Eliane, S. L. Bjorgaard, M. R. Hammond, H. Vitzthum, S. M. Blackmon, D. T. Frederick, M. Hazar-Rethinam, B. A. Nadres, E. E. Van Seventer, S. A. Shukla, K. Yizhak, J. P. Ray, D. Rosebrock, D. Livitz, V. Adalsteinsson, G. Getz, L. M. Duncan, B. Li, R. B. Corcoran, D. P. Lawrence, A. Stemmer-Rachamimov, G. M. Boland, D. A. Landau, K. T. Flaherty, R. J. Sullivan, and N. Hacohen. Resistance to checkpoint blockade therapy through inactivation of antigen presentation. *Nat Commun*, 8(1):1136, 2017.

[176] D. Chowell, L. G. T. Morris, C. M. Grigg, J. K. Weber, R. M. Samstein, V. Makarov, F. Kuo, S. M. Kendall, D. Requena, N. Riaz, B. Greenbaum, J. Carroll, E. Garon, D. M. Hyman, A. Zehir, D. Solit, M. Berger, R. Zhou, N. A. Rizvi, and T. A. Chan. Patient HLA class I genotype influences cancer response to checkpoint blockade immunotherapy. *Science*, 359(6375):582–587, 2018.

[177] M. Lauss, M. Donia, K. Harbst, R. Andersen, S. Mitra, F. Rosengren, M. Salim, J. Vallon-Christersson, T. Torngren, A. Kvist, M. Ringner, I. M. Svane, and G. Jonsson. Mutational and putative neoantigen load predict clinical benefit of adoptive T cell therapy in melanoma. *Nat Commun*, 8(1):1738, 2017.

[178] P. L. Chen, W. Roh, A. Reuben, Z. A. Cooper, C. N. Spencer, P. A. Prieto, J. P. Miller, R. L. Bassett, V. Gopalakrishnan, K. Wani, M. P. De Macedo, J. L. Austin-Breneman, H. Jiang, Q. Chang, S. M. Reddy, W. S. Chen, M. T. Tetzlaff, R. J. Broaddus, M. A. Davies, J. E. Gershenwald, L. Haydu, A. J. Lazar, S. P. Patel, P. Hwu, W. J. Hwu, A. Diab, I. C. Glitza, S. E. Woodman, L. M. Vence, II Wistuba, R. N. Amaria, L. N. Kwong, V. Prieto, R. E. Davis, W. Ma, W. W. Overwijk, A. H. Sharpe, J. Hu, P. A. Futreal, J. Blando, P. Sharma, J. P. Allison, L. Chin, and J. A. Wargo. Analysis of immune signatures in longitudinal tumor samples yields insight into biomarkers of response and mechanisms of resistance to immune checkpoint blockade. *Cancer Discov*, 6(8):827–37, 2016.

[179] R. E. Vilain, A. M. Menzies, J. S. Wilmott, H. Kakavand, J. Madore, A. Guminski, E. Liniker, B. Y. Kong, A. J. Cooper, J. R. Howle, R. P. M. Saw, V. Jakrot, S. Lo, J. F. Thompson, M. S. Carlino, R. F. Kefford, G. V. Long, and R. A. Scolyer. Dynamic changes in PD-L1 expression and immune infiltrates early during treatment predict response to PD-1 blockade in melanoma. *Clin Cancer Res*, 23(17):5024–5033, 2017.

[180] B. Seliger, U. Wollscheid, F. Momburg, T. Blankenstein, and C. Huber. Characterization of the major histocompatibility complex class I deficiencies in B16 melanoma cells. *Cancer Res*, 61(3):1095–9, 2001.

[181] C. A. Janeway, P. Travers, M. Walport, and M. J. Shlomchik. *Immunbiology: The Immune System in Health and Disease*, volume 5th edition of *Immunobiology*. Garland Science, New York, 5th edition, 2001.

[182] E. Schwich, G. T. Ho, J. LeMaoult, C. Bade-Doding, E. D. Carosella, P. A. Horn, and V. Rebmann. Soluble HLA-G and HLA-G bearing extracellular vesicles affect ILT-2 positive and ILT-2 negative CD8 T cells complementary. *Front Immunol*, 11:2046, 2020.

12 Supplemental material

12.1 Supplementary tables

Supplementary Tab. S1: KEGG pathway analysis showing that the pathway of antigen processing and presentation is predicted to be negatively affected in WM266-4 SCG2 OE melanoma cells compared to control (WM266-4 EV) melanoma cells.

Pathway	Direction	Number of genes	p value
Antigen processing and presentation	down	62	0.0916

Supplementary Tab. S2: Gene Ontology pathway analysis listing pathways predicted to be negatively affected in WM266-4 SCG2 OE melanoma cells compared to control (WM266-4 EV) melanoma cells.

Pathway	Direction	Number of genes	p value
antigen processing and presentation of exogenous peptide antigen via MHC class I, TAP-dependent	down	74	0.0028
antigen processing and presentation of peptide antigen via MHC class I	down	94	0.0003
antigen processing and presentation of exogenous peptide antigen via MHC class I	down	77	0.0021
antigen processing and presentation of peptide antigen	down	184	0.0381
antigen processing and presentation of exogenous peptide antigen	down	171	0.0466
MHC protein complex assembly	down	6	0.0173
MHC class I protein binding	down	17	0.0529

Supplementary Tab. S3: Reactome pathway analysis listing pathways predicted to be negatively affected in WM266-4 SCG2 OE melanoma cells compared to control (WM266-4 EV) melanoma cells.

Pathway	Direction	Number of genes	p value
Antigen processing: Ubiquitination and Proteasome degradation	down	302	0.1179
Class I MHC mediated antigen processing and presentation	down	370	0.0458
Antigen Presentation: Folding, assembly and peptide loading of class I MHC	down	25	0.00001

Supplementary Tab. S4: KEGG pathway analysis showing that the pathway of antigen processing and presentation is predicted to be negatively affected in C32 SCG2 OE melanoma cells compared to control (C32 EV) melanoma cells.

Pathway	Direction	Number of genes	p value
Antigen processing and presentation	down	62	0.0001

Supplementary Tab. S5: Gene Ontology pathway analysis listing pathways predicted to be negatively affected in C32 SCG2 OE melanoma cells compared to control (C32 EV) melanoma cells.

Pathway	Direction	Number of genes	p value
antigen processing and presentation of exogenous peptide antigen via MHC class I, TAP-dependent	down	74	0.0013
antigen processing and presentation of peptide antigen via MHC class I	down	94	0.0014
antigen processing and presentation of exogenous peptide antigen via MHC class I	down	77	0.0016
antigen processing and presentation of peptide antigen	down	184	0.0058
antigen processing and presentation of exogenous peptide antigen	down	171	0.0116
MHC protein complex assembly	down	6	0.0050
MHC class I protein binding	down	17	0.0562

Supplementary Tab. S6: Reactome pathway analysis listing pathways predicted to be negatively affected in C32 SCG2 OE melanoma cells compared to control (C32 EV) melanoma cells.

Pathway	Direction	Number of genes	p value
Antigen processing: Ubiquitination and Proteasome degradation	down	302	0.0450
Class I MHC mediated antigen processing and presentation	down	370	0.0749
Antigen Presentation: Folding, assembly and peptide loading of class I MHC	down	25	0.7554

12.2 Supplementary figures

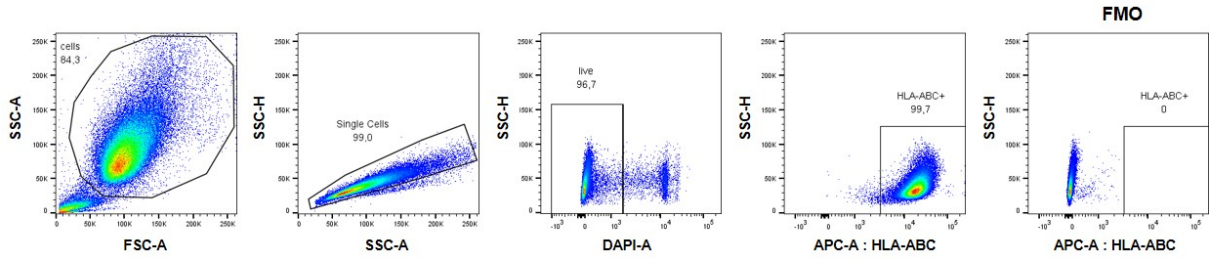

Supplementary Fig. S1: General gating strategy.
General gating strategy used for flow cytometry. Fluorescence minus one (FMO) control was used to set the gate for HLA-ABC$^+$ cells.

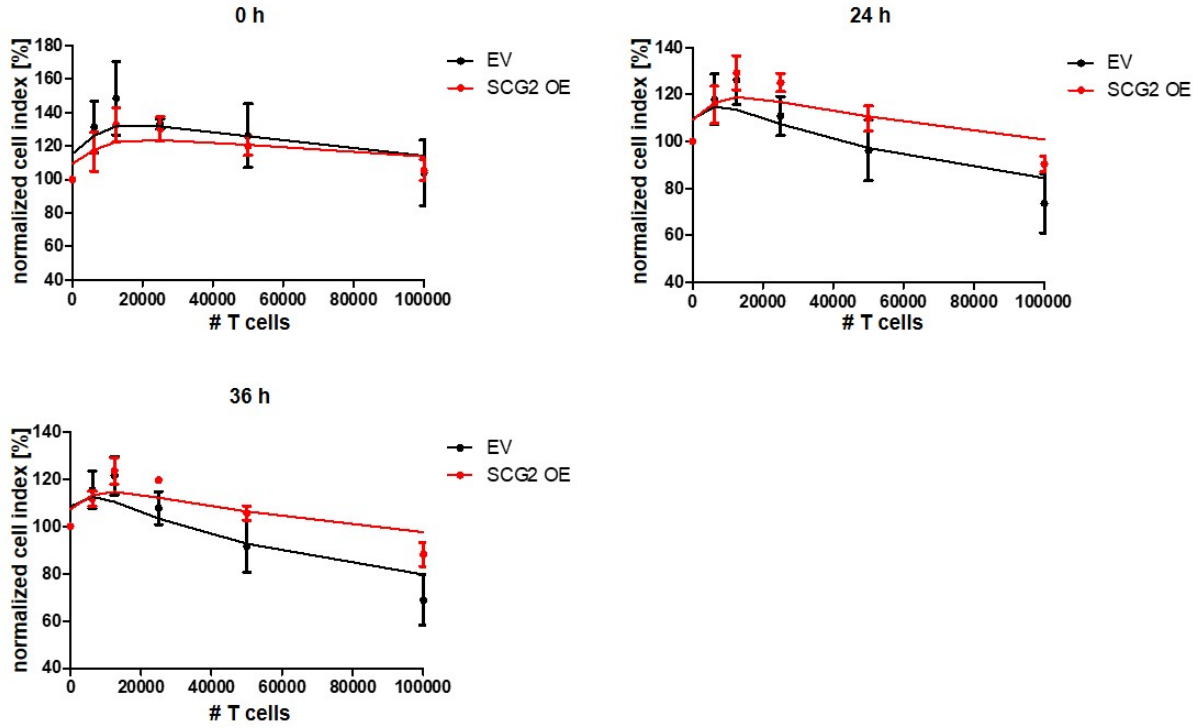

Supplementary Fig. S2: Titration of MART-1-specific T cells.
Determination of the optimal number of T cells for T cell cytotoxicity assay by titration of different amounts (0; 6,250; 12,500; 25,000; 50,000; and 100,000) of MART-1-specific T cells at 0h, 24h, and 36h time point. Comparison of the normalized cell index of EV and SCG2 OE melanoma cells. Normalized cell index was determined by the impedance measured through the interaction of the melanoma cells with the gold biosensors. A decreasing normalized cell index indicates cell killing.

13 Acknowledgement

Herewith I would like to thank **Prof. Dr. Jochen S. Utikal** for not only giving me the opportunity to realize my PhD work in his group at the German Cancer Research Center (DKFZ) but also for his support and guidance throughout my PhD. The last years helped me to develop on the personal and professional level. I am sure that these skills will help me for my future scientific career.

I also want to thank **Prof. Dr. Viktor Umansky** for all his great scientific advises and contributions to my research project whenever it was needed. Additionally, I am also thankful to the lab members of the group of Prof Dr. Viktor Umansky for their support and good advises during the lab meetings. Moreover, I am grateful to my TAC members **Prof. Dr. Jonathan Sleeman** and **PD Daniel Lipka** for their scientific input and advice during my TAC meetings and the interest in my project. Another big thank you goes to **Giovanni** and **Rafael** for taking time to assist me with specific experimental designs and analyses.

My special thanks goes to the whole group of Prof. Dr. Jochen S. Utikal for their help and support in a scientific and personal manner. Especially to my colleagues who became my friends over this journey: **Juliane** and **Daniel**. Thank you so much for all the nice memories and funny moments, which made stressful days much more tolerable and going to work so easy. I am very grateful you accompanied me during all those years and I am very happy to have met you. Another thanks goes to **Marlene P.** and **Jenny** for their help with my experiments, funny stories and conversations. I also want to thank all the former and current lab members, especially **Karol, Laura, Aniello, Sunee, Marlene V., Özge, Sandra, Yiman,** and **Ni-Na** for the nice moments I shared with you.

Moreover, I want to thank **Thomas** for supporting me with the analysis of the microarray data and helping me with every statistical question I had. In this course I also want to thank the Microarray Unit of the Genomics and Proteomics Core Facility and the Flow Cytometry Core Facility of the DKFZ for providing excellent technical assistance and equipment. In addition, I want to thank the NCT-Gewebebank facility of the Pathology Unit of the University of Heidelberg for providing the TMA slide-scanning service.

The biggest thanks goes to my **mother** for her unconditional love, help, and support throughout my life whenever and wherever I needed it. You were always there for me in

any situation in my life. You encouraged me, cheered me up, and believed in me when I was struggling. For all those reasons and many more, I am really grateful to have you and I am happy to say, that in my eyes, I have the worlds' best mum. Besides my mum I am grateful to my **grandma and grandpa** for encouraging me in my professional and personal decisions and for always letting me know that I have their full support. Of course I also want to thank the rest of my **family**, including my aunt, uncle, and cousins, for all their moral support.

Last but not least, I want to thank all of my **friends**, for supporting me, giving me advice, listening to me, and grabbing a beer with me whenever I needed it. All of you made this whole journey so much better and I am very thankful to have you in my life. Here, a very special thanks goes to **Timo**, who made the last years of my PhD, which were the most stressful years, so much easier with just being at my side.

My greatest gratitude goes to each one of you!